Hierarchical Tropical Cloud Systems in an Analog Shallow-Water Model

JUN-ICHI YANO,*,† JAMES C. MCWILLIAMS,# AND MITCHELL W. MONCRIEFF

National Center for Atmospheric Research,@ Boulder, Colorado

KERRY A. EMANUEL

Center for Meteorology and Physical Oceanography, Massachusetts Institute of Technology, Cambridge, Massachusetts

(Manuscript received 31 May 1994, in final form 10 November 1994)

ABSTRACT

Recent observations have revealed an hierarchy of cloud clusters and superclusters within the Madden–Julian oscillation of the equatorial troposphere. The authors here report on the results of simulations with a model based on a simple nonlinear analog of the shallow-water equations. The model consists of a troposphere represented by single values of vertical velocity and temperature and in which the horizontal motions are assumed always to represent the first baroclinic mode. The troposphere overlies a subcloud layer of fixed depth in which the evolution of moist entropy is predicted. The model is driven by specified values of radiative cooling and sea surface temperature, and a Newtonian relaxation of the surface wind toward a specified value. The system is horizontally homogeneous except for an anisotropy owing to the equatorial β effect.

An eastward-propagating low-wavenumber disturbance containing an hierarchy of superclusters and cloud clusters is spontaneously generated from a random initial state using each of three cumulus parameterizations: a Kuo-like scheme and two prognostic schemes. A fourth scheme, which assumes an instantaneous adjustment to convective neutrality, fails to produce an hierarchical structure. Experiments with fixed wind speed in the surface flux formulas demonstrate that the WISHE (wind-induced surface heat exchange) mechanism is responsible for the organized structures in the model fields, except when the Kuo-like scheme is used; even in this case the modes are strongly affected by WISHE.

The supercluster resembles a Matsuno–Gill pattern in all three cases, but the horizontal cloud distribution within the superclusters differs substantially among the three schemes. The Kuo-like scheme produces grid-column convection aligned along the convergence zones as a result of its direct coupling of convection with the large-scale convergence. This scheme always produces grid-scale motions. The prognostic schemes, which allow for the finite timescale of convection, are less prone to gridpoint structure, but the degree of such structure depends sensitively on the parameters of the schemes and the presence or absence of time-lagged downdrafts.

The authors find that the wavenumber spectrum of convective updrafts is nearly flat, while the zonal wind spectrum is strongly peaked at low wavenumbers. This behavior exists even if the nonlinear advection terms are switched off, showing that these play little or no role in the final wavenumber selection. Even turning off all of the model nonlinearity except for the "up-only" nature of convection preserves the essential structure of the full solution, although it does weakly flatten the zonal wind spectrum.

The dependence of the behavior of the system on the magnitude and direction of the background surface wind is also explored. A weaker easterly wind forcing leads to a modulation of the superclusters into a yet lower-wavenumber structure; this modulation propagates faster than the superclusters. Westerly wind forcing suppresses the Kelvin-type mode and generates a mixed mode resembling a mixed Rossby–gravity wave. A further increase of the westerly wind forcing induces westward-moving disturbances as well. This model is considered as a framework for interpreting more complicated tropical models.

1. Introduction

Tropical cloud systems are well known to be organized into an hierarchical structure (see Nakazawa 1988; Yano and Nishi 1989, and the references therein). The largest structures, known as the Madden–Julian wave or 30–60 day oscillation (Madden and Julian 1971, 1972), have scales on the order of 10^4 km and propagate eastward with a phase velocity of about 10 m s^{-1}. There is also evidence of lower levels of structure, consisting of superclusters, having scales of 2000–3000 km, embedded within the Madden–Julian waves and propagating eastward at a faster rate (e.g., Hayashi and Nakazawa 1989),

* UCAR Visiting Scientist Program.

† Current affiliation: CRC-SHM, Monash University, Clayton, Victoria, Australia.

Current affiliation: Institute of Geophysics and Planetary Physics and Department of Atmospheric Sciences, University of California, Los Angeles, Los Angeles, California.

@ The National Center for Atmospheric Research is sponsored by the National Science Foundation.

Corresponding author address: Jun-Ichi Yano, CRC-SHM, Monash University, 8 Redwood Drive, Notting Hill, Victoria 3168, Australia.
E-mail: jiy@vortex.shm.monash.edu.au

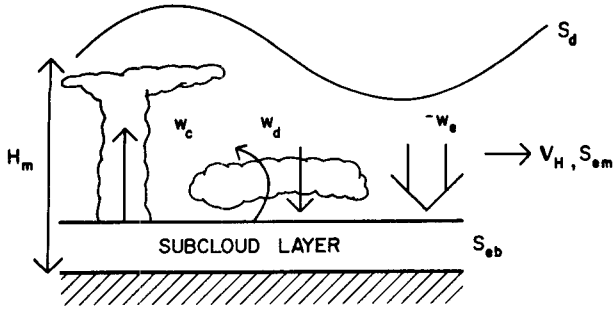

FIG. 1. The model configuration.

and westward-propagating cloud clusters of order 100 km (e.g., Leary and Houze 1979).

Previous large-scale modeling efforts have had some success at simulating various aspects of this hierarchy. A pioneering work is that of Hayashi and Sumi (1986), who removed the land from a standard GCM and used zonally invariant sea surface temperature. Their simulations, which employ a Kuo convective scheme, produce several grid-scale precipitation areas ($\sim 10^3$ km) that propagate eastward with a phase velocity of about 15 m s^{-1}. These are spatially modulated by a planetary-scale structure with a dominant wavenumber 1 ($\sim 10^4$ km), propagating with the same phase velocity as each precipitation area. They identified these structures as superclusters and Madden–Julian waves, respectively, even though the observed Madden–Julian waves propagate slower than the superclusters. Also, in reality the Madden–Julian waves appear to be more nearly a temporal modulation of the superclusters and contain usually only one supercluster [see Fig. 1 of Nakazawa (1988)]. Westward-propagating cloud clusters do not appear in their simulations. The other simulation using a moist convective adjustment scheme did not exhibit this cloud hierarchy (Numaguti and Hayashi 1991).

Lau and Peng (1987) performed several numerical simulations using a Kuo-like convective scheme. Lau et al. (1989) showed that in this model, westward-propagating cloud clusters appear persistently only in the presence of a longitudinal sea surface temperature gradient. However, perhaps owing to the low resolution of the model (rhomboidal truncation to 15 wavenumbers, corresponding to a longitudinal resolution of 7.5°), both the superclusters and the cloud clusters occur at the grid scale (~3000 km). Itoh (1989), using a model similar to that of Lau and Peng, showed that with a higher horizontal resolution (2° in longitude), the hierarchy of superclusters and cloud clusters is spontaneously generated without a longitudinal SST gradient. In his simulation, the grid-scale cloud clusters are clearly embedded in a larger-scale supercluster. Two types of eastward-propagating structures in this model may be identified with the Madden–Julian waves and the superclusters. However, in contrast with observations, the slowly propagating supercluster does not have a larger horizontal scale than the fast-propagating superclusters. One goal of the present work is to extend Itoh's simulation to even higher resolution so as to resolve more details of the hierarchical structure.

Our main purpose here is to attempt to delineate the dynamics of the various elements of the hierarchy, using a model of vastly simplified vertical structure but high horizontal resolution, and to explore the sensitivity of the model results to the type of convective representation used.[1] The model is designed to simulate the broad range of spatial and temporal scales involved in tropical atmospheric dynamics, evident, for example, in fractal horizontal structure of clouds (e.g., Lovejoy 1982; Yano and Takeuchi 1987). We wish to assess the possibility that the rich spectrum of tropical motions arises from the nonlinear interaction of large-scale flows with convective processes.

In accordance with this view, we perform simulations of high horizontal resolution and drastically reduce the vertical degree of freedom by retaining only the first baroclinic mode. This results in a system of equations that is analogous to the shallow-water system (Yano and Emanuel 1991). We do not impose any spatial inhomogeneity on the system, apart from the gradient of the Coriolis parameter $f = \beta y$, in order to demonstrate spontaneous generation of a disturbance hierarchy out of random initial conditions. Specifically, we assume homogeneity of both the sea surface temperature and the radiation, which consists of a uniform forcing plus a Newtonian cooling (we neglect cloud/cloud-free radiation differences for the sake of simplicity). We include the effects of subgrid-scale convective downdrafts, wind-dependent surface evaporation, cumulus heating, and moistening of the troposphere, and an explicit thermodynamic budget in the subcloud layer. We will use and compare several different cumulus parameterization schemes and will comment on their effectiveness.

The model formulation, presented in section 2, is the same as that of Yano and Emanuel (1991), apart from retention of the nonlinear terms, the exclusion of the stratosphere, and the use of alternative convective schemes. The system is initialized with random perturbations and is numerically integrated with time. We describe the initialization and other numerical aspects of the model in section 3, present the main results in section 4, report on some supplemental experiments and analyses of the results in section 5, and discuss the results in section 6.

2. Model formulation

The framework (Fig. 1) is essentially a one-and-a-half-layer model: a dynamically active free troposphere

[1] A similar problem has been addressed by Chao and Lin (1994) using a longitudinally one-dimensional GCM with a high vertical resolution. The advantage of their approach is being able to test various full-GCM cumulus parameterizations and potentiality to examine the nonlinear interactions of vertical modes.

and a dynamically passive subcloud layer. The wind $\mathbf{v}_H$ defined at the top of the subcloud layer is driven by the pressure gradient determined from the dry entropy (S_d) of the midlevel troposphere. The total entropy, a measure of the system moisture, is calculated in the subcloud layer and in the middle troposphere. These entropies are S_{eb} and S_{em}, respectively. The subgrid-scale cloud effects are represented by the convective updraft vertical velocity w_c and the downdraft vertical velocity w_d. The environmental subsidence outside of the cumulus areas is represented by w_e.

Thermodynamic variables (S_d, S_{eb}, S_{em}) are defined as fluctuating components on a constant pressure surface, so that only their relative values have meaning (cf. section 3). For convenience, we normalize the entropy by heat capacity, so that fluctuations in S obey

$$\delta S_d \approx \delta\theta/\theta_0,$$

with $\theta_0 = 300$ K, where θ is the potential temperature.

The details of the model formulation are presented in the following subsections. For brevity, definitions of the symbols are given in the appendix, along with the chosen values of physical constants.

a. Model dynamics

The dynamics on an equatorial β plane are reduced to an analog of the shallow-water system by assuming a first-mode baroclinic vertical structure. The momentum equation, evaluated at the top of the subcloud layer, contains a Rayleigh wind forcing:

$$\frac{D}{Dt}\mathbf{v}_H = -\nabla\delta\phi - \beta y\hat{\mathbf{k}}\times\mathbf{v}_H - \frac{C_D}{h}|\mathbf{v}_H|\mathbf{v}_H - \frac{1}{\tau_D}(\mathbf{v}_H - \mathbf{v}_0), \quad (2.1)$$

with the time derivative defined by

$$\frac{D}{Dt} \equiv \frac{\partial}{\partial t} + u\frac{\partial}{\partial x} + v\frac{\partial}{\partial y}.$$

The Rayleigh forcing is a relaxation toward a uniform velocity $\mathbf{v}_0 = (u_0, 0)$ on a timescale τ_D; it replaces the large-scale dynamics of the mean tropical circulation. Here C_D is the surface drag coefficient and h is the constant depth of the subcloud layer. The perturbation geopotential ($\delta\phi$), which corresponds to fluctuations of depth in the shallow-water system, is related to the dry entropy S_d (characterizing the midtroposphere temperature) by

$$\delta\phi = -C_p\gamma\epsilon T_b S_d. \quad (2.2)$$

This relation is derived by vertically integrating the hydrostatic equation, using thermodynamic relations and the constraint that the mass-weighted vertically averaged velocity perturbations vanish, so that only the first baroclinic mode is retained in the system (Emanuel 1987; Yano and Emanuel 1991). Here γ is the ratio of moist- to dry-adiabatic lapse rates, ϵ is a thermodynamic efficiency, and T_b is the absolute temperature at the top of the subcloud layer. The continuity of mass is given by the incompressible approximation integrated from the top of the subcloud layer to the middle troposphere over the depth H_m:

$$\nabla\cdot\mathbf{v}_H + \frac{w}{H_m} = 0, \quad (2.3)$$

where w is a representative vertical velocity of the troposphere. The effect of density stratification is accounted for by implicitly introducing a log$p$ coordinate, so that the vertical scales H, H_m are density-weighted values.

b. Thermodynamics

The effects of convection on the large-scale thermodynamics are expressed in terms of the convective mass flux averaged over the fractional area σ_c occupied by cumuli in a given grid domain. This is represented by a cumulus vertical velocity w_c using the incompressible approximation to mass continuity. By conservation of the total vertical mass flux,

$$w = \sigma_c w_c + (1 - \sigma_c)w_e, \quad (2.4)$$

where w_e is the large-scale descent averaged over the fractional area $1 - \sigma_c$. Note that w_c represents an ensemble-average convective updraft velocity.

1) DRY ENTROPY

The equation for the dry entropy of the troposphere is given by

$$\frac{D}{Dt}S_d = -\frac{N^2}{g}w + \dot{Q}_{\text{conv}} - \dot{Q}_R, \quad (2.5)$$

where $\dot{Q}_{\text{conv}} = \sigma_c w_c[N^2/g + \epsilon_k(S_{eb} - S^*_{em})/H]$ is the cumulus heating and $\dot{Q}_R = \dot{Q}_{R0} + S_d/\tau_R$ the longwave radiation, expressed in terms of a Newtonian cooling. The switching parameter ϵ_k is set equal to 1 in the Kuo-like scheme [see section 2c(4)], otherwise to 0.

The second term in $\dot{Q}_{\text{conv}}$ represents the heating according to the Kuo-like scheme specialized to the limited vertical structure of our model. (Note that the cloud mass flux $\sigma_c w_c$ is also replaced by w when using the Kuo-like scheme.) In the two-layer formulation, there is essentially no difference between a Kuo scheme and the "explicit" release of conditional instability by the large-scale motion, save that all updrafts are assumed to be saturated. The vertical advection term outside clouds is expressed as $w_e N^2/g = wN^2/g - \dot{Q}_{\text{conv}}$. We note that the system consisting of (2.1)–(2.3) and (2.5) with no heating has a first baroclinic mode phase speed given by

$$c = N\left(C_p\gamma\epsilon T_b\frac{H_m}{g}\right)^{1/2} \approx 50 \text{ m s}^{-1}.$$

2) SUBCLOUD LAYER

The tropical subcloud layer represents a conduit through which heat and moisture pass from the sea surface to cumulus clouds. In strict quasi-equilibrium conditions, there is a one-to-one relationship between the subcloud-layer entropy and the tropospheric virtual temperature (Emanuel 1987). Prediction of the subcloud-layer entropy is the critical thermodynamic consideration in our model. Heat enters the subcloud layer from the sea surface and exits through the top by the agents of mean subsidence and the downdrafts.

The supply of heat from the ocean is described by a bulk aerodynamic formula:

$$E = C_\theta |\mathbf{v}_H| (S^*_{eb} - S_{eb}), \tag{2.6}$$

where S^*_{eb} is the saturation entropy of the sea surface. Convective activity cools and dries the subcloud layer chiefly through the downdrafts (D_d) both on the scale of the cumulus and the shallow clouds, and through the large-scale descent (D_L) between the clouds. We assume that both effects exchange the equivalent entropy of the subcloud layer (S_{eb}) and of the troposphere (S_{em}) at a rate given by a measure of downdraft magnitude w_d and the large-scale descent w_e, respectively:

$$D_d = \sigma_d w_d (S_{eb} - S_{em}), \tag{2.7a}$$

$$D_L = -(1 - \sigma_c) w_e^{\downarrow} (S_{eb} - S_{em}) \tag{2.7b}$$

and

$$D = D_d + D_L, \tag{2.8}$$

where

$$w_e^{\downarrow} = \begin{cases} w_e, & w_e < 0 \\ 0, & w_e > 0. \end{cases}$$

Here σ_d is the fractional area covered by the downdrafts. Additionally, in the case of the Kuo-like scheme, we subtract the term

$$C = \sigma_c w_c (S_{eb} - S^*_{em}) \tag{2.9}$$

from the entropy budget of the subcloud layer, to be consistent with the latent heating term in $\dot{Q}_{\text{conv}}$ [see Eq. (2.5)].

With these effects accounted for, the equation for the subcloud-layer equivalent entropy S_{eb} is given by

$$h \frac{D}{Dt} S_{eb} = E - D - \epsilon_k C, \tag{2.10}$$

where h is the depth of the subcloud layer.

3) MIDLEVEL EQUIVALENT ENTROPY

The tendency equation for the total entropy S_{em} representing the middle troposphere is defined such that the total entropy integrated over the troposphere satisfies the conservation law

$$\frac{D}{Dt}(hS_{eb} + HS_{em}) = E - H\dot{Q}_R. \tag{2.11}$$

By subtracting Eq. (2.10) from Eq. (2.11), we obtain

$$H \frac{D}{Dt} S_{em} = D - H\dot{Q}_R + \epsilon_k C. \tag{2.12}$$

c. Cloud representations

The convective updraft and downdraft velocities, w_c and w_d, respectively, remain to be determined. We experiment with simplified versions of four types of cumulus parameterizations in this model. Two schemes (a, d) are *diagnostic* in Arakawa and Chen's (1986) terminology, while the other two (b, c) are *prognostic* in the sense that the cumulus convection has a memory.

1) STATISTICAL EQUILIBRIUM

In strict quasi equilibrium, as defined by Arakawa and Schubert (1974), the cumuli are assumed to consume available energy at exactly the rate at which it is supplied by large-scale processes, and the available energy for each cloud type remains invariant. In that case, there is a one-to-one correspondence between the entropy of the subcloud layer and the temperature of the free troposphere. In terms of the present model formulation, this is expressed as

$$S_{eb} - \gamma S_d = 0, \tag{2.13}$$

unless the system is stable to convection. The constraint (2.13), coupled with (2.5) and (2.10) and an expression relating the downdraft to the updraft velocities, diagnostically defines the cumulus mass flux. This closure has been used in WISHE (wind-induced surface heat exchange) models (Emanuel 1987; Yano and Emanuel 1991). To complete the closure, the convective downdraft mass flux $\sigma_d w_d$ is assumed to be proportional to the total cumulus mass flux $\sigma_c w_c$:

$$\sigma_d w_d = \frac{1 - \epsilon_p}{\epsilon_p} \sigma_c w_c, \tag{2.14}$$

with the proportionality defined in terms of the precipitation efficiency ϵ_p (Yano and Emanuel 1991), which is set to 0.9 in the present study.[2]

2) DYNAMIC ADJUSTMENT

The concept of exact statistical equilibrium is physically sound as long as the grid size is sufficiently large

[2] With help of Eq. (2.14), the total cumulus mass flux may be written as $\sigma_c w_c = (\sigma_c/\epsilon_p) w_c - \sigma_d w_d$ with the sum of the cumulus updraft $(\sigma_c/\epsilon_p) w_c$ and the convective downdraft $\sigma_d w_d$, whereas σ_c/ϵ_p may measure a *total* cumulus fractional area, also taking into account a portion of the cumulus area not contributing in a grid-scale average due to a cancellation by downdrafts.

that the dynamical timescales are much longer than the cumulus timescale. However, once we start to decrease the grid size sufficiently, or the cloud systems are of a mesoscale character, the timescale separation implicitly assumed in this scheme is not strictly valid. Emanuel (1993) found that large-scale dynamics are sensitive to the small but finite timescales of convection. Thus, we explicitly consider a finite timescale for the (buoyant) cumulus growth.

In this scheme, we assume that the cumulus parcel is accelerated by the buoyancy force (Durran and Klemp 1982; Emanuel 1983; Yano and Emanuel 1991):

$$B = C_p\Gamma_m(S_{eb} - \gamma S_d), \tag{2.15}$$

where Γ_m is the moist-adiabatic lapse rate. Following parcel theory, the pressure gradient in the cloud-scale momentum equation is ignored, resulting in

$$\left(\frac{\partial}{\partial t} + \mathbf{v}_H\cdot\nabla + w_c\frac{\partial}{\partial z}\right)w_c = B.$$

We approximate vertical advection by

$$w_c\frac{\partial}{\partial z}w_c \approx w_c^2/2H,$$

assuming that the cumulus towers all extend to the tropopause. The final expression is

$$\left(\frac{\partial}{\partial t} + \mathbf{v}_H\cdot\nabla\right)w_c = B - w_c^2/2H. \tag{2.16}$$

The closure (2.14) for the convective downdrafts is also used in this scheme. We set $w_c = 0$ whenever it becomes negative. The scheme anticipates that the cumulus updraft kinetic energy $w_c^2/2$ is equal to the convective available potential energy HB (= CAPE) in the homogeneous equilibrium state when the left-hand side of Eq. (2.16) vanishes.

3) Grid-column scheme

In this scheme, the convection is represented as a prognostic process within a grid column: the convection is activated at, say, $t = t_0$, when the buoyancy force exceeds the threshold B_c, which is defined as a critical buoyant energy necessary to initiate cumulus towers occupying a fractional area σ_c. The cumulus updraft velocity, which is set to $w_c = 0$ at the initial time, grows according to

$$\frac{\partial}{\partial t}w_c = B \tag{2.17}$$

until the buoyancy force B becomes negative at, say, $t = t_1$. A finite buoyancy B_c is required for the onset of parameterized cumulus convection, to represent the physical prerequisite of finite vertical displacements of air parcels to overcome typical stability of air just above the boundary layer. We introduce only a small critical buoyancy $\theta_0 B_c/C_p\Gamma_m \approx 10^{-2}$ K, taking into account the small cumulus fractional area σ_c assumed in the present series of experiments (some experiments were repeated with $B_c = 0$, and no difference was found).

At the time $t = t_1$, we set $w_c = 0$ so that the convection instantaneously turns into mesoscale downdrafts, which decay exponentially with a timescale τ_d:

$$w_d = (w_c + w_d)(t = t_1 -)e^{(t_1-t)/\tau_d}. \tag{2.18}$$

During the cumulus growth period, we assume that there is also a downdraft given by

$$w_d = \frac{1-\epsilon_p}{\epsilon_p}w_c + w_d(t = t_0)e^{(t_0-t)/\tau_d}. \tag{2.19}$$

The first term on the right-hand side represents a cumulus-scale downdraft and the second a mesoscale downdraft whose value is $w_d(t = t_0)$ at the onset of convection.

Equation (2.17) is chosen primarily by virtue of its simplicity (the advection terms are omitted). The exponential decay of the mesoscale downdrafts in Eqs. (2.18)–(2.19) is inspired by the observational analysis by Zipser (1969) and others [see, e.g., Houze (1989) for a review] that tropical squall line systems are accompanied by mesoscale downdrafts that persist for several hours after the termination of deep convection.

Since the cumulus activity is represented as a grid-scale process in this scheme, we may need to adjust the cumulus fractional area σ_c with changes of the grid scales. However, we do not consider this possibility in the present paper.

4) Modified Kuo scheme

We introduce a Kuo-like scheme by setting $\sigma_c w_c = w$ when $w > 0$ and $S_{eb} - S_{em}^* > 0$ in Eqs. (2.5), (2.10), and (2.12) with $\epsilon_k = 1$. Convection is absent when neither of the above conditions is satisfied at a grid point.

According to the hypothesis of Kuo (1974), the heating by an ensemble of convective cloud is proportional to the horizontal convergence of water vapor flux in an atmospheric column. This quantity is not Galilean invariant, however, and Krishnamurti et al. (1976, 1980) proposed a small modification that addresses this defect. According to their formulation, the vertically integrated convective heating is proportional to

$$-L_v w\frac{\partial q}{\partial z},$$

where L_v is the latent heat of vaporization. Adding and subtracting a term proportional to $\partial\theta/\partial z$, the convective heating applied to our simple model may be expressed as

$$Q_{\text{conv}} = w[N^2/g + (S_{eb} - S_{em})/H], \tag{2.20}$$

applied only where the quantity is positive *and* the atmosphere is conditionally unstable. The above formulation assumes 100% precipitation efficiency [so that $\epsilon_p = 1.0$ in Eq. (2.14): Kuo's b parameter = 0]. To account for reduced precipitation efficiency and to eliminate discontinuities in the convective heating, we replace (2.20) with

$$Q_{\text{conv}} = w[N^2/g + (S_{eb} - S^*_{em})/H], \quad (2.21)$$

where $S^*_{em} = \gamma S_d$. This formulation eliminates discontinuities in the effective static stability that occur in the Kuo formulation; thus this scheme should not be as noisy as the Kuo scheme.

3. Computational design

The equations are integrated on an equatorial β plane with dimensions $(20\,700 \text{ km})^2$, corresponding to a half-earth plane (a fractional difference of computational values from a round number here and elsewhere is only due to a nondimensionalization in the code) and an assumed tropospheric depth of 20 km [this corresponds to a density-weighted vertical scale of $H = 8$ km (cf. appendix)]. The domain is bounded in latitude by rigid walls and has periodic boundary conditions in the longitudinal direction. The equator is set at the middle of the domain ($y = 0$). We use 128×129 points over the domain with a grid spacing of $\Delta x = \Delta y = 161$ km. (Note that one additional grid point is required in the latitudinal direction to apply the sidewall boundary conditions.)

We adopt a pseudospectral method: the horizontal gradients of the variables are computed in Fourier space, and all the remaining computations are done on grid points. For dealiasing, we apply the "2/3 rule" (Orszag 1971) to each variable (except for w_c and w_d in the statistical equilibrium and the grid-column schemes) in conjunction with the computations of the horizontal gradients, so that any Fourier components with wavenumbers larger than 42 in either direction are omitted at each time step. A leapfrog time integration with a time step $\Delta t = 2.69$ min is used. The time averaging is applied every 10 steps to eliminate the computational mode and to maintain numerical stability (Matsuno 1966b).

The integration is initialized with a random distribution of dry entropy fluctuations, with a variance of $\langle S'^2_d \rangle^{1/2} = 0.6$ K, where $S'_d = S_d - \langle S_d \rangle$ and the brackets represent the domain mean value. We assume no wind, no cloud, and a stable troposphere initially. All the other variables are assumed homogeneous, that is, $S_{eb} = S_{em} = 0$ with a constant component $\langle S_d \rangle = 1.8$ K for the dry entropy. Hence, the numerical integration represents an adjustment to a statistical equilibrium state.

4. Results: Standard case

a. Grid-column scheme

We first present results of the integrations using the grid-column scheme, because they are representative of most of the other schemes summarized in the next subsection.

The initial evolution of the downdraft mass flux $\sigma_d w_d$ is presented in Fig. 2, which also shows the wind vectors $\mathbf{v}_H$. The spontaneous generation of a large-scale pattern from the random initial condition is evident.

Convective instability is induced by the combined effects of the entropy increase in the subcloud layer

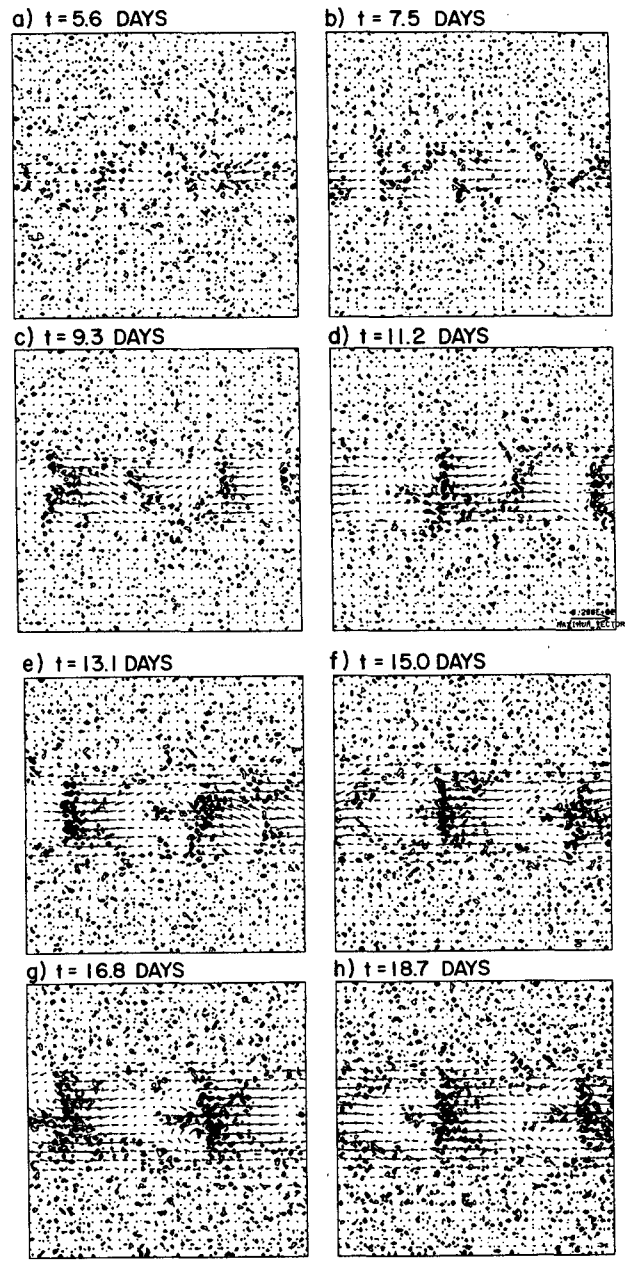

FIG. 2. The temporal evolution of the downdraft field using the grid-column adjustment scheme from (a) $t = 5.6$ days with an interval of 1.87 days to (h) $t = 18.7$ days. The contour interval for the downdraft $\sigma_d w_d$ is 6×10^{-3} m s^{-1} from 0 to 0.15 m s^{-1}. The unit of the wind speed, 5 m s^{-1}, is shown at the lower right of (d).

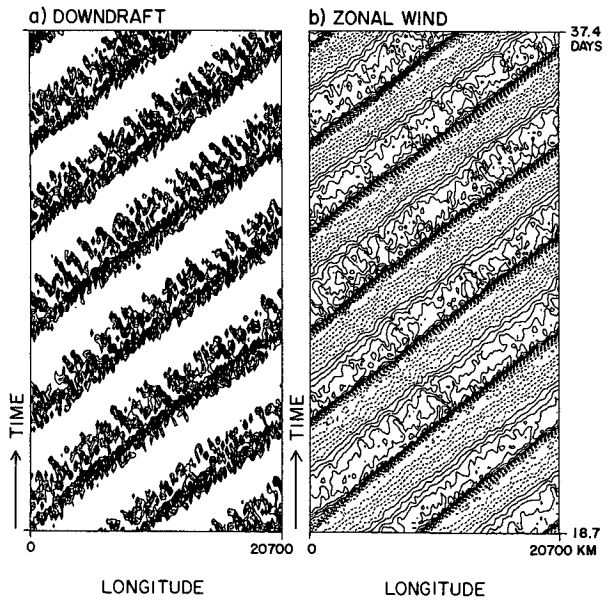

FIG. 3. Time–longitude section of a mean between 1.45°S and 1.45°N from t = 18.7 days to 37.4 days for (a) the downdraft $\sigma_d w_d'$ and (b) the zonal velocity u' with the zonal means subtracted. The contour interval is 3×10^{-3} m s^{-1} and 0.5 m s^{-1} in (a) and (b), respectively. Only positive values are drawn in (a), while the negative contours are represented by dashed lines in (b). Westward-propagating cloud clusters are embedded in eastward-propagating superclusters.

due to the wind-induced surface heat flux and the constant cooling of the troposphere by longwave radiation. An additional tropospheric cooling by adiabatic ascent accompanying the disturbances finally initiates convective activity. The clouds are initially distributed homogeneously over the domain (t = 3–6 days) but subsequently organize along the equator in conjunction with the development of an equatorially confined easterly wind (Fig. 2a).

By day 7 the cloud system is organized into about five clusters along the equator (Fig. 2b). After day 8 four clusters are evident (Fig. 2c), but one dies out at day 10 (Fig. 2d). The remaining three clusters remain stable until the weakest is absorbed as it is overtaken by a larger one at day 13, as they propagate eastward (Fig. 2e). Two superclusters eventually form (Fig. 2f) and persist for the remainder of the integration period (56.1 days); this is essentially the final state of the integration.

The pattern of flow around the superclusters (Fig. 2h, also Fig. 5d) is similar to the linear, shallow-water response to a moving heat source (Chao 1987), which extends the earlier analyses of a stationary source [Matsuno–Gill pattern: Matsuno (1966a), Gill (1980)]: there is a strong easterly wind region to the east of the supercluster and a cyclone pair to the west.

An equatorial time–longitude section of the perturbation downdraft mass flux and zonal velocity during a later stage of evolution (t = 18.7–37.4 days) is shown in Fig. 3. The perturbations are deviations from the zonal mean. The phase relationship between the maximum cloud activity and the convergence is evident in this figure. We further note that westward-propagating clusters are embedded within eastward-propagating superclusters. Nakazawa (1988, Fig. 2) discovered this phenomenon in OLR data analysis and called it an "hierarchical structure."

In order to see the relationship between the supercluster and the cloud clusters more clearly, we plot the downdraft mass flux and zonal wind fields at a 4.48-h interval in Fig. 4. As the superclusters propagate eastward, a series of cloud clusters are shed to their rear. The cloud clusters decay as they propagate westward, and new cloud activity, which may be interpreted as new cloud clusters, is initiated at the leading edge of the superclusters. In this respect, the supercluster is a modulated train or family of cloud clusters.

b. Results with other schemes

A comparison of the results with different schemes is summarized in Fig. 5, which displays the final state of the cloud and the wind fields.

The case with the strict statistical equilibrium scheme (Fig. 5a) is the exception: it does not generate a planetary-scale pattern evident in the other schemes. The final state exhibits eight pairs of westward-propagating cloud clusters aligned along the equator. The clusters do not experience a coalescence associated with the grid-column scheme. Although eastward-propagating clusters are generated initially, these turn into westward-propagating modes by day 10. The in-

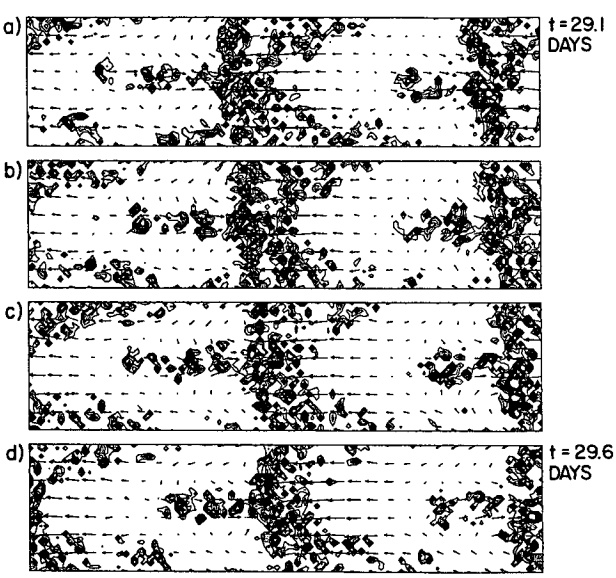

FIG. 4. The evolution of cloud clusters embedded within the supercluster shown with 4.48-h interval from (a) t = 29.1 days to (d) t = 29.6 days. The downdraft and the wind fields are represented in the same manner as in Fig. 2 but between 22.5°S and 22.5°N.

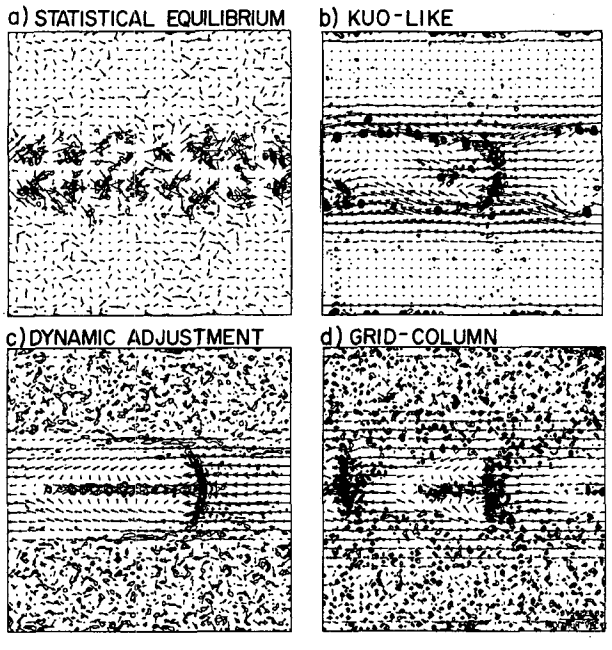

FIG. 5. The mature stage of the cloud field with (a) the statistical equilibrium (t = 22.4 days), (b) the Kuo-like (at t = 35.5 days), (c) the dynamic-adjustment (t = 31.8 days), and (d) the grid-column schemes (t = 37.4 days). The downdraft $\sigma_d w_d$ is shown with an interval of 3×10^{-3}, 6×10^{-4}, and 6×10^{-3} m s^{-1} in (a), (c), and (d), respectively; the cumulus updraft $\sigma_c w_c$ is shown in (b) with the interval 6×10^{-3} m s^{-1}. Note that the minimum contour is 6×10^{-4} m s^{-1} in (c). The unit wind vector (shown at the lower right) is 5 m s^{-1} for (a), (c), and (d) but 7.5 m s^{-1} for (b).

ability of the strict statistical equilibrium scheme to produce planetary wave activity is consistent with the linear analysis of Emanuel (1993).

The remaining three cases have a strikingly similar structure despite the different cloud parameterization schemes. In all three cases, a coherent pattern is organized principally as a consequence of a series of cloud-cluster coalescences.

The organizational stage, during which cloud clusters form, lasts longest for the Kuo-like case, in which cloud clusters do not appear until day 15. The coalescence process is, in contrast, shorter in the Kuo-like case than the case with two other schemes, because five well-defined clusters are already conspicuous by day 17. Only three clusters survive after day 19, and by this time, the strongest already features a Matsuno-Gill pattern. Two weaker clusters appear off the equator by day 26.

In contrast, the dynamic-adjustment scheme requires the shortest time to organize well-defined clusters. Seven clusters identified at day 6 decrease to four clusters by day 8. Only the strongest one survives until day 18.

Details of the convection patterns do, however, substantially differ among the various schemes. In the Kuo-like scheme case (Fig. 5b), the supercluster consists of a conglomerate of single gridpoint cumuli consistent with its direct coupling with the large-scale vertical velocity (e.g., Emanuel 1988). These gridpoint cumuli are aligned along the convergence zones. On the other hand, the dynamic–adjustment scheme (Fig. 5c) produces a smooth cloud field containing only large-scale structure within the supercluster. Note that in this scheme the cumuli are considered in an ensemble-mean sense, so they tend not to produce any single-grid structure. However, note a strong longitudinal concentration of the superclusters in the neighborhood of the convergence zone.

The structure of the grid-column case (Fig. 5d) is by and large intermediate to the two previous cases: as in the Kuo-like scheme case, it consists of a conglomerate of single-grid-column cumuli. However, due to the lack of direct coupling with the large-scale vertical velocity in this scheme, the cumuli are even more homogeneously spread than in the case of the dynamic-adjustment scheme.

Time–longitude sections similar to these shown in Fig. 3 are presented for the dynamic-adjustment and the Kuo-like schemes in Fig. 6 and 7, respectively. The dynamic-adjustment case (Fig. 6) represents a very similar hierarchical structure to that of the grid-column scheme. A major difference is the narrower spacing between the clusters within the supercluster, so that it contains more clusters than the grid-column case. On the other hand, the Kuo-like scheme (Fig. 7) is characterized by a sporadic westward detachment of clusters from the superclusters. This type of feature with the Kuo-type scheme was also obtained by Itoh (1989).

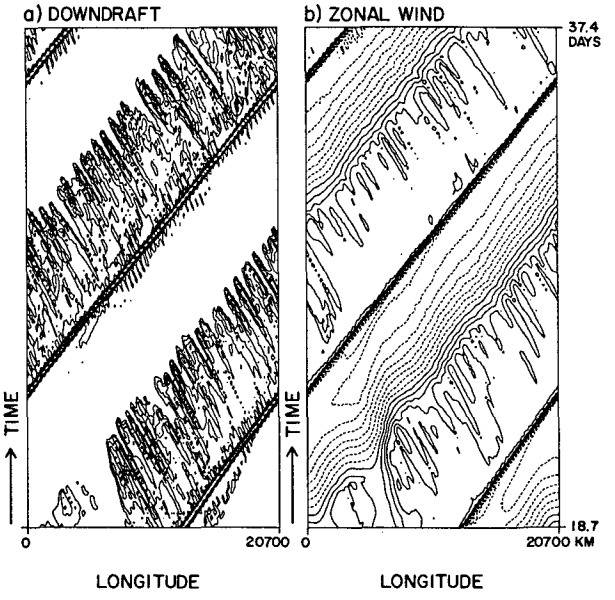

FIG. 6. The same as Fig. 3 but for the dynamic-adjustment scheme. The contour interval for the downdraft in (a) is changed to 6×10^{-4} m s^{-1}.

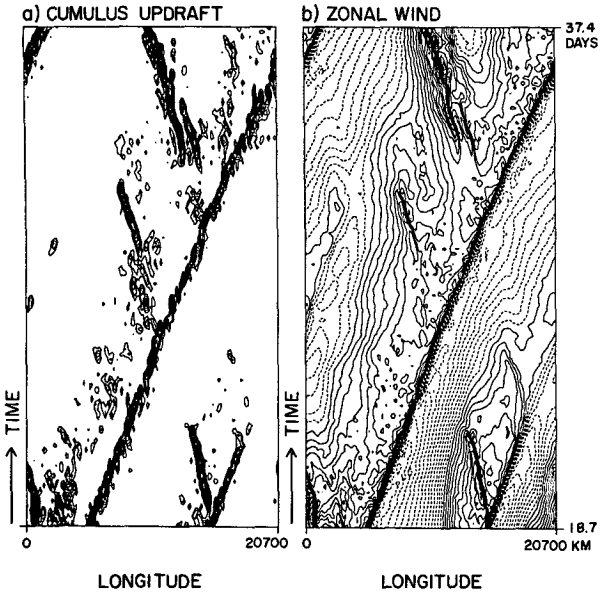

FIG. 7. The same as Fig. 3 but for the Kuo-like scheme. The cumulus velocity is instead shown in (a) with the interval 6×10^{-3} m s^{-1}.

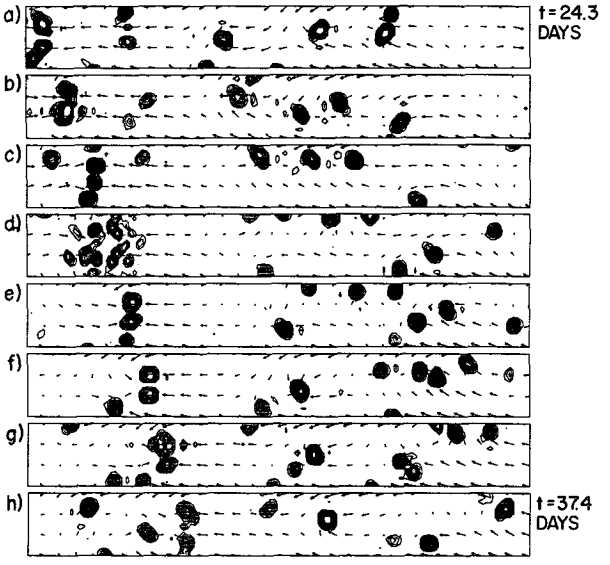

FIG. 8. The Kuo-like scheme result without WISHE process: the cumulus field is plotted from (a) $t = 24.3$ days to (h) $t = 37.4$ days with an interval of 1.87 days. The contour interval is 6×10^{-3} m s^{-1} and the unit wind vector length is 2.5 m s^{-1}. The area from 7.23°S to 7.23°N is shown.

5. Analysis

a. Wave–CISK versus WISHE

Perhaps the best-known theory for tropical wave motions is wave–CISK (see, e.g., Lindzen 1974), in which the large-scale, low-level convergence is directly coupled to the cumulus activity, so that convective available potential energy (CAPE) is directly converted into large-scale kinetic energy. However, recent work by Emanuel (1993), Brown and Bretherton (1995), and Neelin and Yu (1994) suggests that convection tends to *damp* large-scale motions in the Tropics, if it responds over a finite time to large-scale forcing. These authors argue that only the WISHE mechanism, represented by Eq. (2.6), and forcing from outside the Tropics can excite large-scale tropical disturbances. On the other hand, linear analyses with Kuo-type schemes, which tend to alias conditional instability onto the resolved scales, show the development of explicit structure even in the absence of wind-dependent surface fluxes. To determine the dynamics underlying the organized structures found in the present model, we undertake a series of experiments in which the WISHE mechanism is turned off at various stages.

1) DECAY EXPERIMENT

In the first set of experiments, we turned off the WISHE process at $t = 37.4$ days by replacing $\mathbf{v}_H$ with the constant $\mathbf{v}_0$ in the heat–moisture exchange term in standard experiments, so that

$$E = C_\theta |\mathbf{v}_0| (S^*_{eb} - S_{eb}), \qquad (5.1)$$

and also set $C_D = 0$ to suppress the subsequent decay of the free waves. In the dynamic–adjustment scheme case, the westward-propagating clusters suddenly disappear and the eastward-propagating supercluster gradually decays over about 15 days. A zone of strong horizontal convergence is emitted westward from the supercluster as soon as the WISHE process is turned off and propagates with a phase velocity of ≈ -10 m s^{-1} along the equator. This is interpreted as a free equatorial Rossby wave. This result may be compared with Fig. 7 of Hayashi and Sumi (1986), where solutions without convection are shown.

The supercluster decays more slowly in the Kuo-like scheme case: it takes 15 days to become intermittent, but then lasts another 10 days. Interestingly, the super-

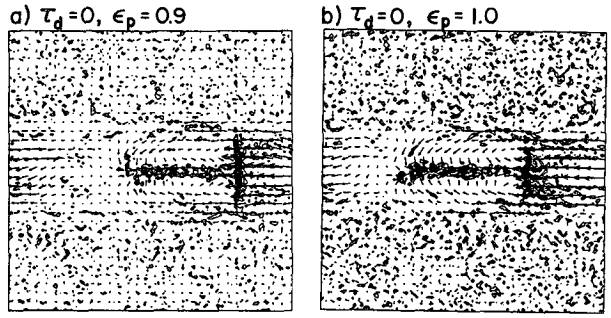

FIG. 9. The grid-column scheme in the limit $\tau_0 \to +0$ at $t = 16.9$ days with (a) $\epsilon_p = 0.9$ and (b) $\epsilon_p = 1.0$. The cumulus updraft $\sigma_c w_c$ is plotted with an interval of 6×10^{-3} m s^{-1}, and the wind vectors with unit of 5 m s^{-1} (cf. Figs. 2, 5).

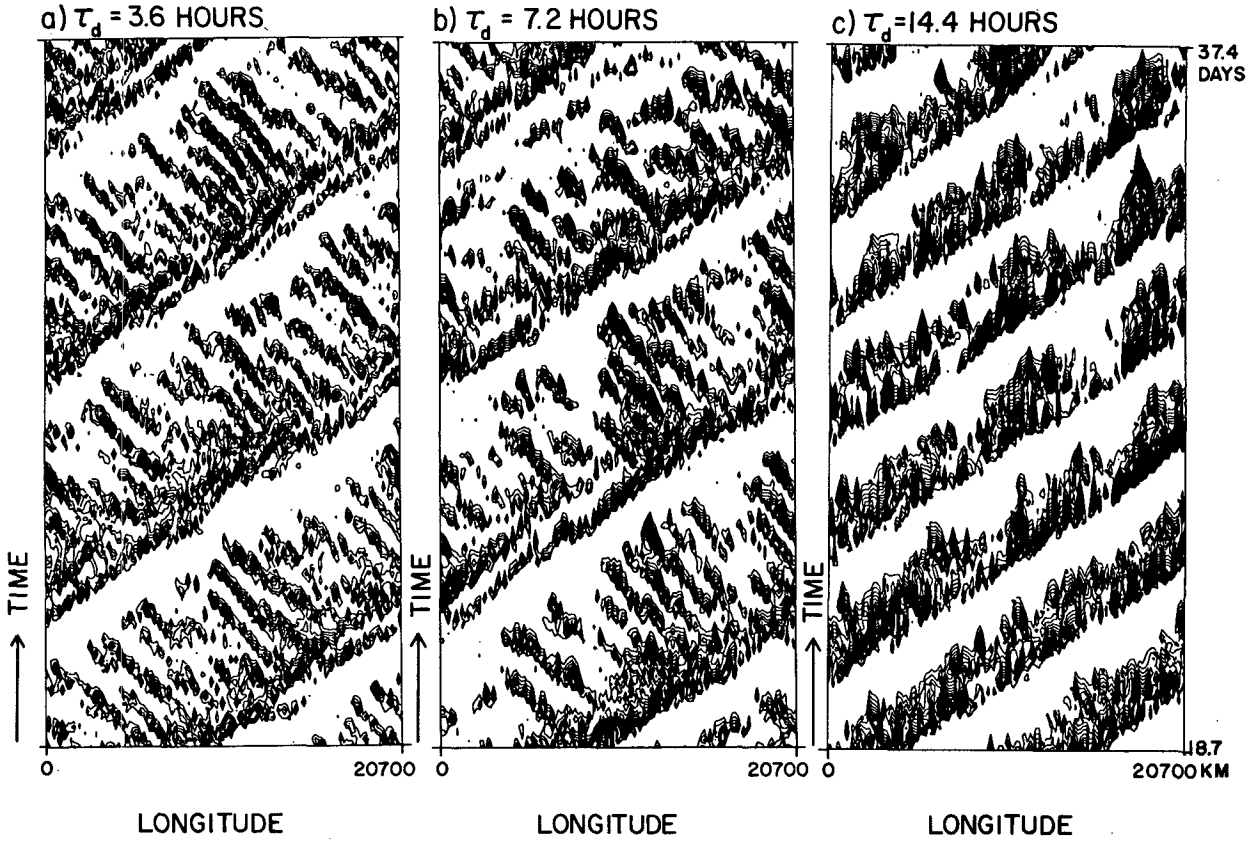

FIG. 10. The dependence of the grid-column scheme on the mesoscale downdraft decay time τ_d: time–longitude section of a mean between 1.45°S and 1.45°N from t = 18.7 to 37.4 days for the downdraft $\sigma_d w_d$ with the contour interval 6×10^{-3} m s^{-1}: (a) τ_d = 3.6 h (twice of the standard value), (b) τ_d = 7.2 h, and (c) τ_d = 14.4 h.

cluster starts to propagate about half as fast 10 days after the WISHE mechanism is switched off. The Rossby wave emission is not as conspicuous with the Kuo-like scheme as it is with the dynamic-adjustment scheme.

The most dramatic change occurs with the grid-column scheme: the whole domain is filled with small-scale convection within a few hours after turning off the WISHE process. This breakdown apparently stems from decaying mesoscale downdrafts remaining after the termination of the convection.

2) EXPERIMENT WITHOUT WISHE

In this experiment, the wind dependence of the surface heat exchange is removed from the beginning of the experiment [the surface friction C_D is retained in this set of experiments so that a possibility of frictional wave–CISK (cf. Wang 1988) is not excluded]. No organized structure is generated either with the dynamic–adjustment or the grid-column scheme. The domain is covered by convection in a few days, but the cumulus activity decays within a few days with the dynamic-adjustment scheme.

On the other hand, the Kuo-like scheme is capable of generating planetary-scale coherent structures even without the WISHE mechanism (Fig. 8). The convection consists of a single, isolated eastward-propagating supercluster (left part of the frame) and an aggregation of superclusters propagating eastward (right part of the frame). The latter may be compared with the results of Hayashi and Sumi (1986, Figs. 3, 4). Each supercluster is confined to only a single gridpoint, in contrast to the control case with wind-dependent surface fluxes. Also, the westward propagating modes are completely missing, as in the results of Hayashi and Sumi.

The results of these experiments are consistent with previous numerical simulations and linear stability analyses: prognostic convective schemes, which respond to available buoyant energy over a finite but small timescale, lead to damping of all resolved disturbance modes in the Tropics. The WISHE mechanism can amplify disturbances. Kuo-type schemes, on the other hand, directly alias conditional instability onto the resolved scales, and in models such as ours with simple vertical structure, there is essentially no distinction between the use of the Kuo-type scheme and direct release of conditional instability by the resolved flow (except that upward motion is *assumed* to be contained in saturated clouds). This aliasing of conditional instability

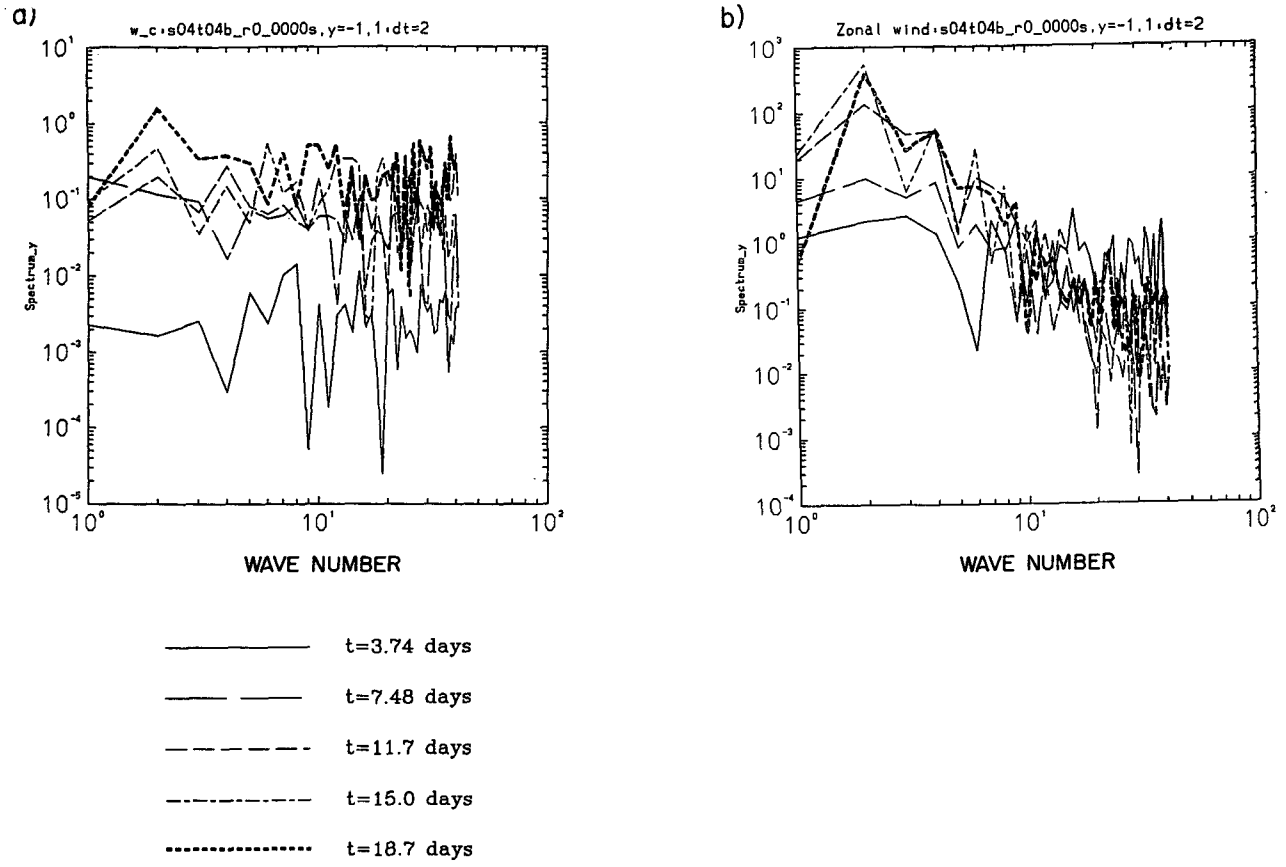

FIG. 11. The power spectra (in nondimensional units) of the standard run with the grid-column scheme as a function of the longitudinal wavenumber for (a) the cumulus velocity w_c and (b) zonal wind u at t = 3.74 days (solid line), 7.48 days (long-dashed line), 11.2 days (dashed line), 15.0 days (chain–dot line), 18.7 days (thick, short-dashed line) averaged over 1.45°S–1.45°N.

onto the resolved scales does lead to Kelvin wave–like structure, even in the absence of WISHE.

b. *Effects of downdrafts*

Downdrafts are an essential element of moist convection and are well known to have a profound influence on the moist entropy of the subcloud layer. Linear stability analysis (e.g., Yano and Emanuel 1991) shows that the phase speed of WISHE modes is sensitive to the assumed precipitation efficiency, which governs the relative magnitude of the downdrafts. Here we present the results of several experiments designed to explore the sensitivity of the model disturbance properties to parameters controlling downdrafts.

In the first experiment, we explore the effects of the finite timescale of downdraft development in the grid-column scheme by setting τ_d to zero in (2.19); this eliminates decaying mesoscale downdrafts. The result, with a finite convective downdraft (ϵ_p = 0.9, Fig. 9a), is to produce fields that look very similar to those of the dynamic-adjustment scheme. This suggests that the principal difference between the schemes is not the Galilean invariance of the dynamic-adjustment scheme but the lagged mesoscale downdraft that we included in the grid-column scheme. Even when the cloud-scale downdrafts are completely turned off (ϵ = 1.0, Fig. 9b), the results are similar. This demonstrates that eastward propagation occurs even when there are no cloud-scale downdrafts, consistent with linear stability analyses (e.g., Emanuel 1987).

The dependence of the simulations with the grid-column scheme on the decay scale τ_d of the mesoscale downdrafts is also investigated (Fig. 10). When the decay timescale of the downdraft is doubled (Fig. 10a), the equilibrium state exhibits a single eastward-propagating coherent structure. Another doubling of the timescale (Fig. 10b) tends to disorganize the cloud-cluster field. On further doubling the decay timescale (Fig. 10c), the configuration with two superclusters is recovered, but the westward propagating cloud clusters are virtually suppressed.

c. *The role of nonlinearity*

How much of the spectrum of tropical motions is due to direct excitation of instabilities at various

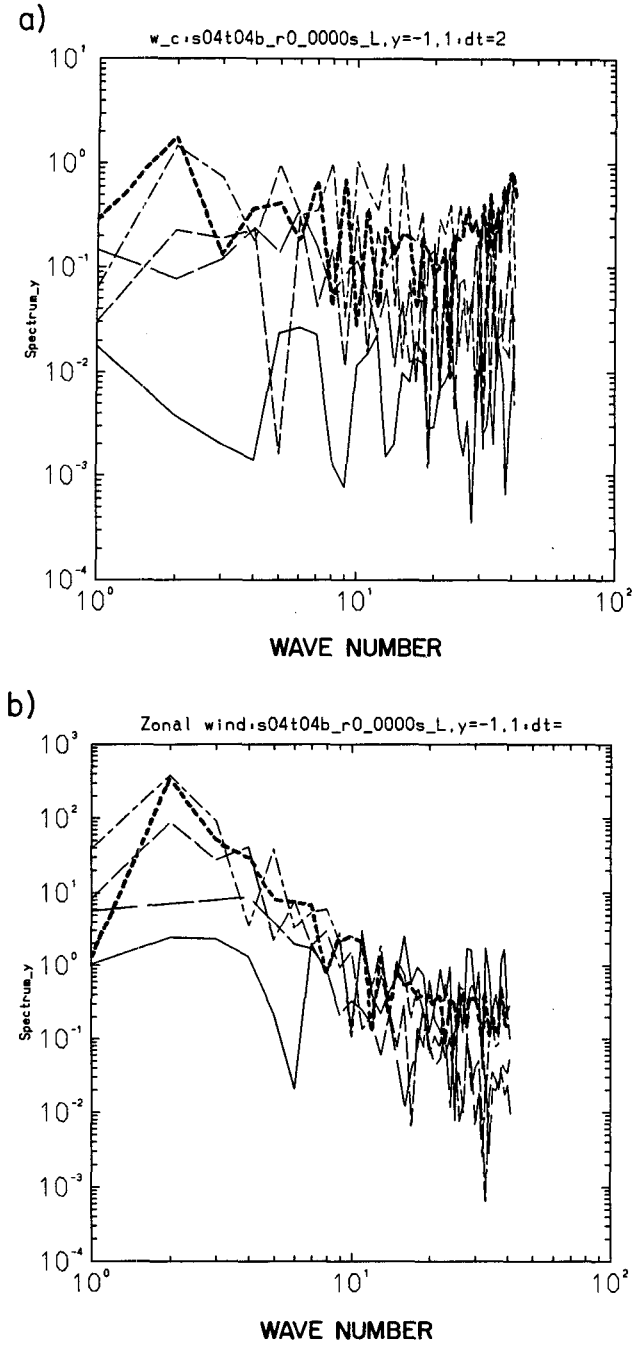

FIG. 12. The same as in Fig. 11 but for the run without advection terms.

scales, and how much results from nonlinear interactions among the directly excited components? For example, what is the mechanism controlling the coalescence of cloud clusters (Fig. 2)? In an attempt to answer this question using the present model, we have performed a number of experiments in which the degree of nonlinearity of the equations is progressively reduced.

1) FULLY NONLINEAR SYSTEM

In order to assess the role of the nonlinearity in establishing the equilibrium states of the model, we have evaluated the temporal evolution of the power spectra of several model fields. To accomplish this, each variable is averaged over 1.45°S–1.45°N, then a Fourier decomposition is made in the longitudinal wavenum-

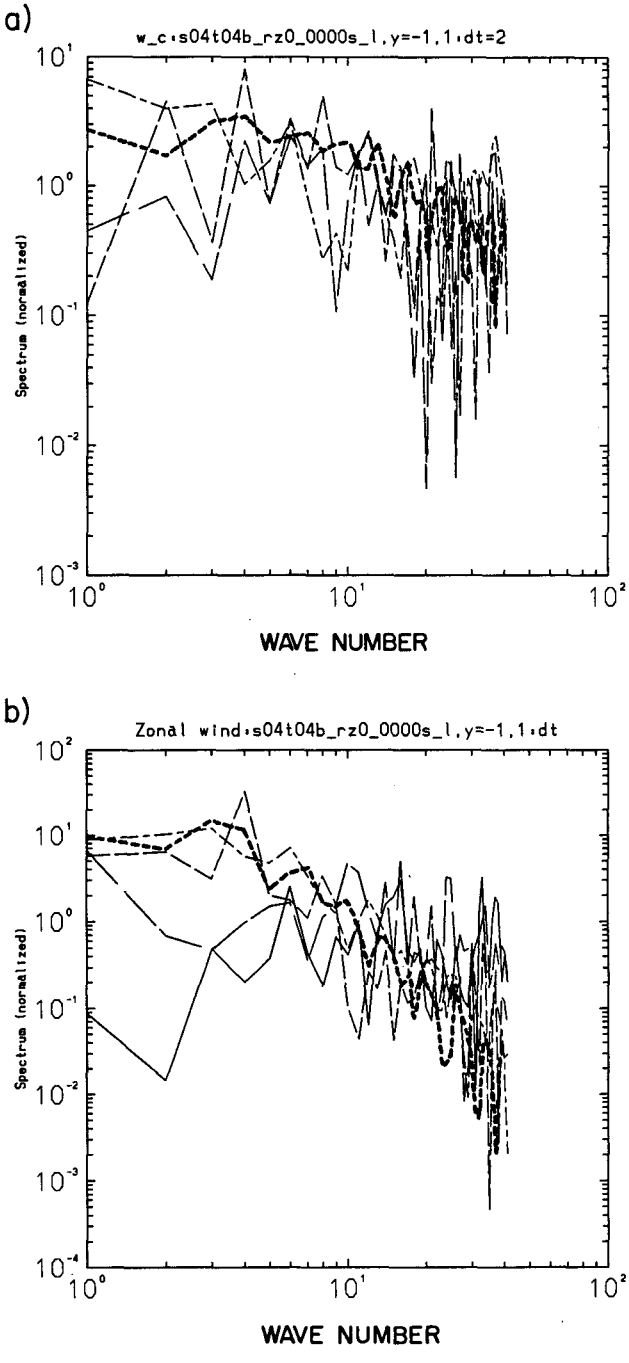

FIG. 13. The same as in Figs. 11 and 12 but for the pseudolinear system. Also the scale is normalized in this figure.

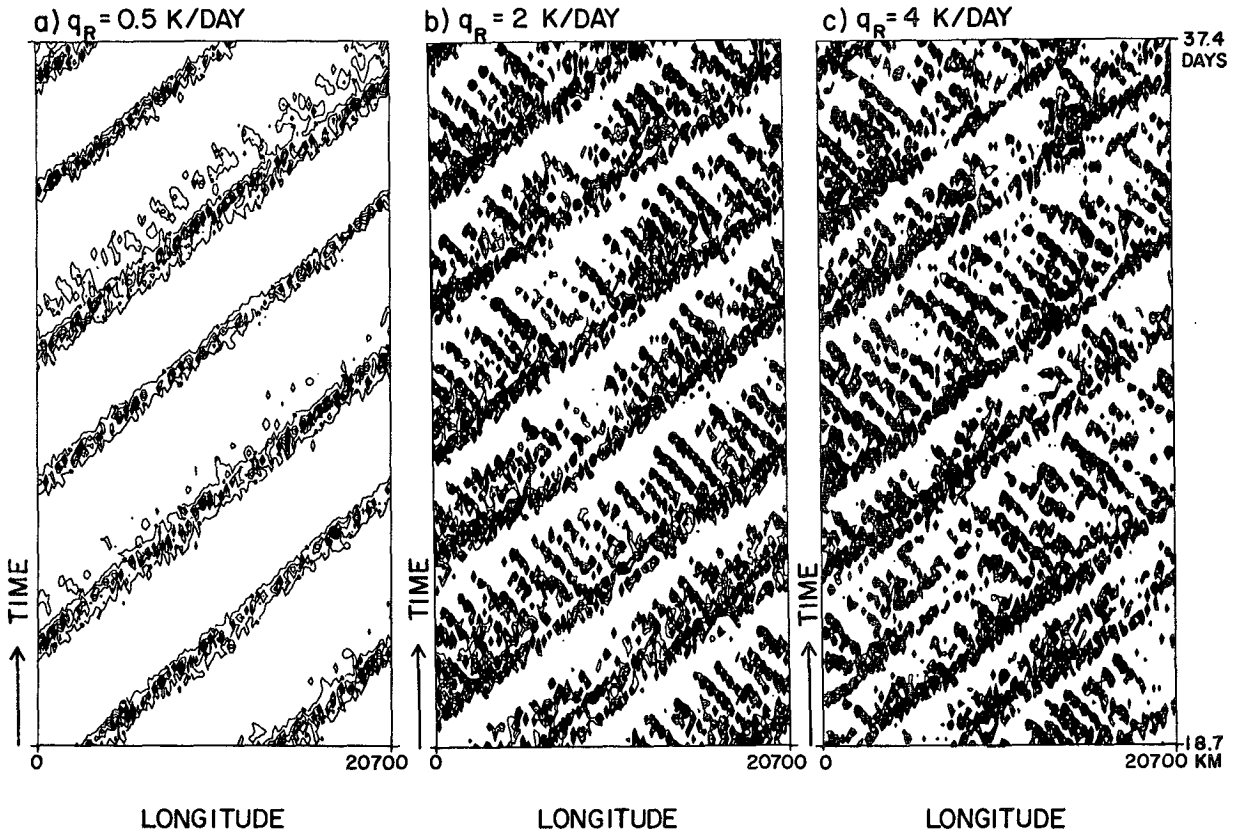

FIG. 14. The dependence of the grid-column scheme on the radiative forcing $\dot{Q}_{R0}$: time–longitude section of a mean between 1.45°S and 1.45°N from t = 18.7 to 37.4 days for the downdraft $\sigma_d w_d$ with the contour interval 6×10^{-3} m s^{-1}. (a) $\dot{Q}_{R0}$ = 0.5 K day^{-1} (half the standard value), (b) $\dot{Q}_{R0}$ = 2 K day^{-1} (twice the standard value), and (c) $\dot{Q}_{R0}$ = 4 K day^{-1} (four times the standard value).

bers. The power is defined as a square of the magnitude of each longitudinal Fourier component.

The evolution of the power spectra of the cumulus vertical velocity w_c and the zonal wind u in the grid-column version of the model is plotted in Figs. 11a and 11b, respectively, at 3.74-day intervals. Early in the simulation (t = 3.74 days, solid curve) the maximum power in the convection spectra is found at wavenumber 8, but it is not a single peak as expected from the linear stability analysis, perhaps reflecting residual noise from the random initial condition. The power spectrum of the convection subsequently evolves into a white spectrum. A peak at wavenumber 2 is noticeable at the final time (t = 15.0 days, dotted curve), but the peak does not persist long after this time (cf. t = 18.7 days, chain–dot curve). The zonal wind spectra (Fig. 11b) starts with a white spectrum shape, but energy eventually accumulates at lower wavenumbers with a slight decrease of energy at higher wavenumbers late in the integration. The power spectra evolve in a similar way with both the Kuo-like and the dynamic-adjustment schemes.

2) THE SYSTEM WITHOUT ADVECTION TERMS

To assess the role of the nonlinearity, we perform a numerical experiment that is identical to the grid-column case described in *a* above, but omitting the advection terms (i.e., D/Dt in all the equations is replaced by $\partial/\partial t$). The nonlinearities that remain are the switch in the convection scheme, vertical entropy flux terms, and the nonlinear surface drag. The evolution of the spectra with time for this case is shown in Fig. 12. The character of the evolution of the spectra is remarkably similar to the fully nonlinear case (Fig. 11). The appearance of the fields in real space is also essentially the same as in the standard case, and the phase velocities of the superclusters and cloud clusters are within a few percent of those of the standard case.

We conclude that advection plays essentially no role in establishing the properties of the equilibrated state in the model. The same experiment is repeated using both the dynamic-adjustment and Kuo-like schemes, and the same conclusion is reached.

3) A PSEUDOLINEAR SYSTEM

In a final experiment, we eliminate all of the nonlinearity in the system aside from the switch in the grid-column convection scheme, starting from an initial condition that represents the zonal average of the equilibrated fully nonlinear system [using the result with 32

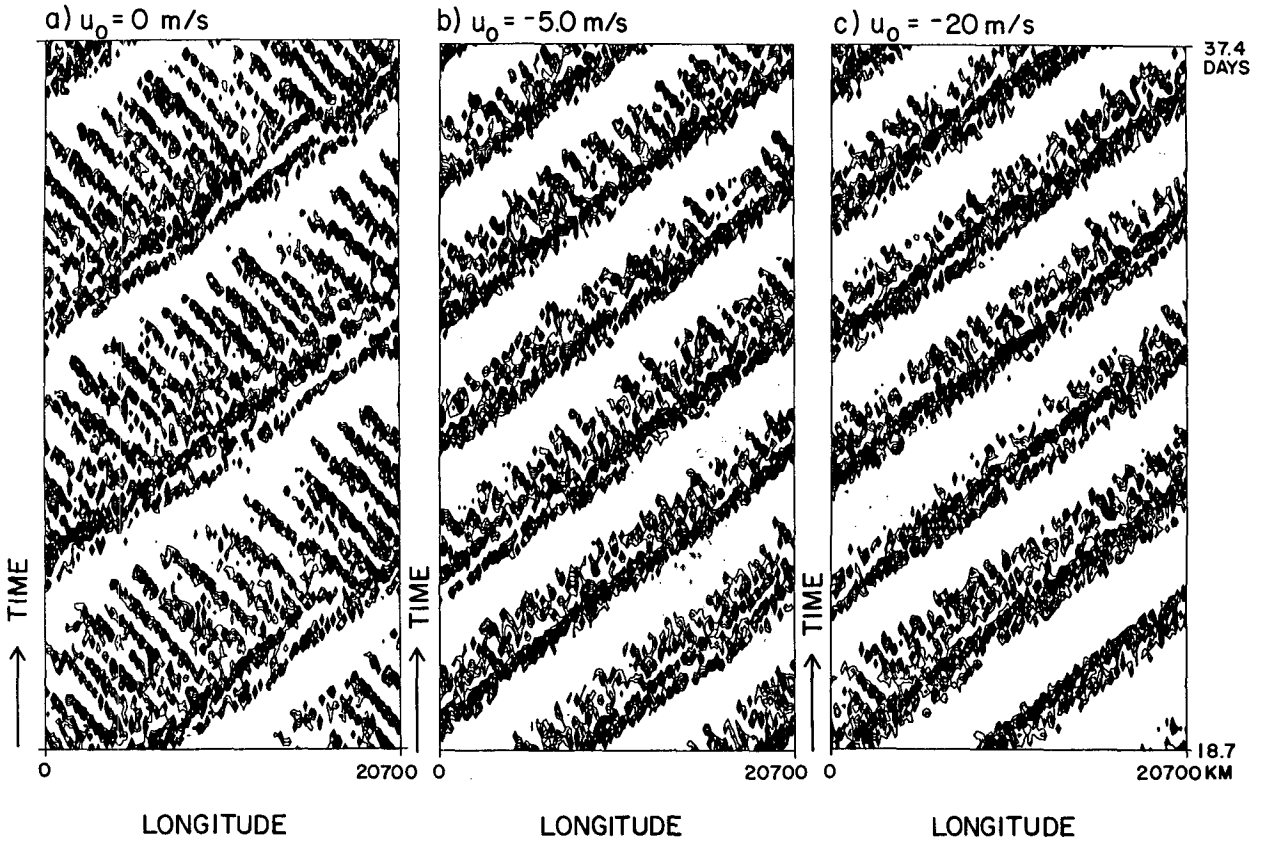

FIG. 15. The dependence of the grid-column scheme on the easterly Rayleigh wind forcing u_0: time–longitude section of a mean between 1.45°S and 1.45°N from t = 18.7 to 37.4 days for the downdraft $\sigma_d w_d$ with the contour interval 3×10^{-3} m s^{-1}. (a) $u_0 = 0$ m s^{-1} (no wind forcing), (b) $u_0 = -5.0$ m s^{-1} (half the standard value), and (c) $u_0 = -20$ m s^{-1} (twice the standard value).

$\times$ 33 resolution described in section 5e(1)]. This results in disturbances that grow exponentially in time. The power spectra (Fig. 13) are normalized so that the power integrated over wavenumber remains constant.

The resulting spectra are remarkably similar to the fully nonlinear integration, except that the zonal wind curve is flatter at low wavenumbers. This appears to indicate that the coalescence process of the cloud clusters was controlled by an implicit nonlinearity owing to the switch in the convective scheme.

d. Effects of radiation and mean wind forcing

Linear theory (e.g., Emanuel 1993) predicts that the growth rate of small-amplitude disturbances is proportional to the degree of air–sea thermodynamic disequilibrium mean state; this is in turn proportional to the radiative cooling rate and inversely proportional to the mean surface wind speed. Linear theory also contains no Kelvin-like modes if the mean wind is westerly, though higher-order modes are not ruled out.

We performed experiments in which the radiative cooling and the direction and speed of the mean wind forcing are varied. We found, in accordance with linear theory, that the eastward-propagating superclusters exist through a large range of cooling rates and wind forcings, as long as the latter are easterly. The westward-propagating clusters weaken if the mean sea–air disequilibrium is reduced either by decreasing the radiative cooling (Fig. 14) or by increasing the mean wind forcing (Fig. 15). These cloud clusters virtually disappear if the radiative cooling is too weak (Fig. 14a) or the mean wind forcing is too strong (Fig. 15c). The superclusters continue to exist even in the absence of mean wind forcing (Fig. 15a), consistent with the recent results of Xie et al. (1993a,b).

Once a westerly wind forcing (i.e., $u_0 > 0$) is set, however, a qualitatively different behavior appears (Figs. 16, 17). With a weak westerly wind forcing (u_0 = 3–7 m s^{-1}), the eastward-propagating Kelvin-type mode is totally suppressed, as expected from linear analysis, but the westward-propagating mode is prominent (Fig. 16a). An intertropical convergence zone (ITCZ)-like cloud band oscillates around the equator, accompanied by pairs of cyclones and anticyclones straddling the equator (Fig. 17a), which is identified as a mixed Rossby–gravity mode from S_d field. Increasing the westerly wind forcing ($u_0 > 8$ m s^{-1}) causes the ITCZ-like cloud band to dissipate (Fig. 17b), and some eastward-propagating disturbances ap-

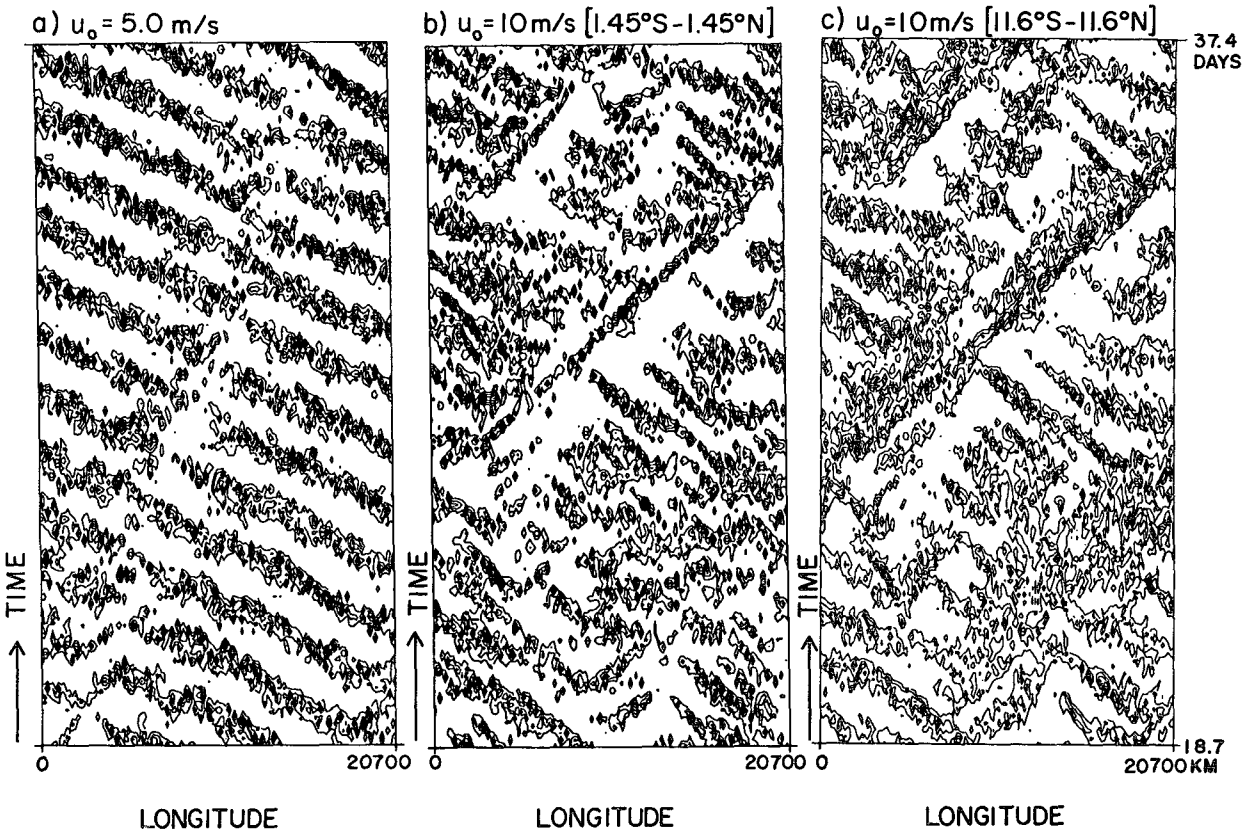

FIG. 16. The dependence of the grid-column scheme on the westerly Rayleigh wind forcing u_0: time–longitude section of a mean between 1.45°S and 1.45°N from t = 18.7 to 37.4 days for the downdraft $\sigma_d w_d$ with the contour interval 6×10^{-3} m s^{-1}. (a) u_0 = 5.0 m s^{-1} and (b) u_0 = 10 m s^{-1}. (c) The same as (b) but of a mean between 11.6°S and 11.6°N with the contour interval 3×10^{-3} m s^{-1}.

pear (Fig. 16b). The hierarchy of the superclusters and the cloud clusters is reestablished to a certain extent. The superclusters propagate more slowly than in the standard case, and there also appears a modulation of the westward-propagating clusters propagating eastward at about half of the phase velocity of the superclusters. This slowly propagating modulation is more clearly seen when a wider latitudinal average is used (Fig. 16c). The overall behavior is more intermittent with a higher westerly wind forcing.

e. *Other sensitivity experiments*

1) RESOLUTION DEPENDENCE

To explore the sensitivity of the simulations to spatial resolution, we also ran the model with all but the statistical equilibrium convection scheme with doubled resolution (so that Δx = 80.5 km), starting from t = 37.4 days and continuing for another 9.35 days.

In the case of the two prognostic convective schemes, the solutions are virtually identical, save for a slight increase in the eastward phase speed of superclusters in the case with the dynamic adjustment, a general sharpening of the edges of cloud clusters, and a decrease in the noise level in the solutions.

Changes in the results of the Kuo-like scheme on doubling the resolution are much more noticeable (Fig. 18). The size of the superclusters decreases and their phase speed increases by 25%. After 6 days, the difference in the overall structure of the supercluster is remarkable (Fig. 18b). This is consistent with the view of the Kuo scheme as a means of aliasing conditional instability onto the resolved scales. The resulting instability has strong components on the grid scale and is thus sensitive to grid size.

One more set of experiments was performed in which the resolution was decreased to 32 × 33; this gives a grid size of roughly two Rossby radii. The integration was carried on for 122 days. No organized structure is generated in runs using any of the convective schemes, due to the poor resolution.

2) DEPENDENCE ON INITIAL CONDITIONS

The standard computations were started from a state far from statistical equilibrium; thus, the timescale to reach equilibrium does not reflect the true timescales in the system. To more accurately determine the equil-

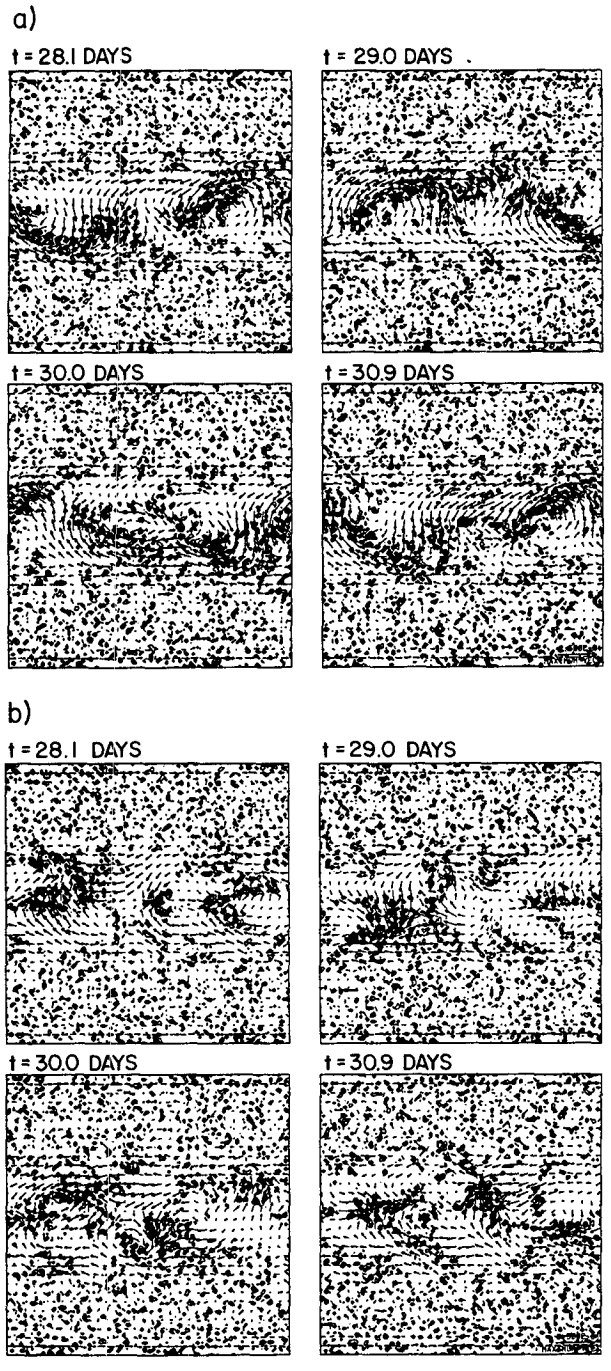

FIG. 17. (a) The same as in Fig. 2 but with $u_0 = 5$ m s^{-1}, from t = 28.1 to 30.9 days with an interval of 0.94 day: the frame is from the upper left to the right and then to the lower left. (b) The same as in Fig. 17a but with $u_0 = 10$ m s^{-1}.

ibration timescale of the system, we performed an additional set of experiments at full resolution, starting from the equilibrated state of the low-resolution run described in the previous subsection. Since this state does not contain any disturbances, it can be considered to be a state of one-dimensional radiative–convective equilibrium. The cloud hierarchy is reestablished over about 10 days with all three parameterizations. The generation timescale of the superclusters is much shorter than in the standard cases and is comparable to the observed genesis timescale of disturbances propagating eastward from the Indian Ocean to the Pacific (cf. Nakazawa 1988).

With the Kuo-like and the dynamic-adjustment schemes, a virtually identical final state is obtained. In the case with the grid-column scheme, however, the final state of the system is different: the superclusters are *spatially* modulated into a single eastward-propagating coherent structure (Fig. 19, compare with Fig. 4), which constitutes a higher order in the hierarchy. The superclusters are successively generated at the front side and decay into a cloud cluster at the rear side of the higher-order coherent structure, so that the modulation is propagating faster than the superclusters. Note, on the other hand, that the observed Madden–Julian waves are identified as *temporal* modulations, propagating slower than the superclusters.

3) DEPENDENCE ON PARAMETERS OF CONVECTIVE SCHEMES

It is of some interest to determine the sensitivity of the simulations to unknown or poorly known parameters in the convection schemes. In the case of the dynamic-adjustment scheme, a decrease of the fractional updraft area σ_c tends to smooth the convection

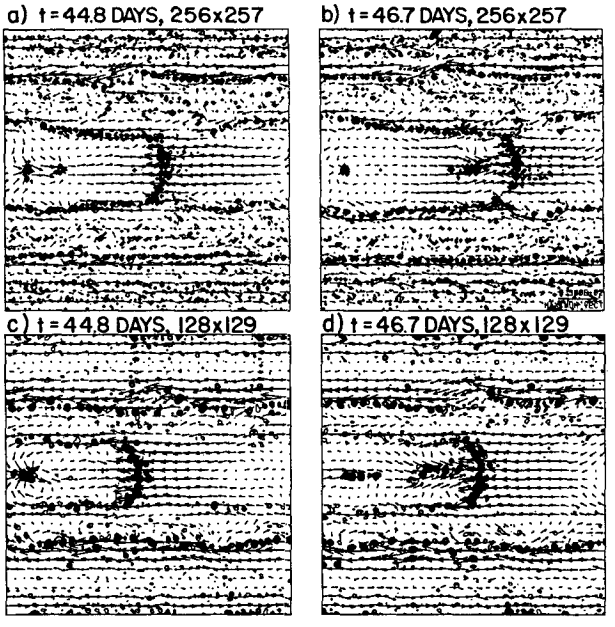

FIG. 18. The resolution dependence of the Kuo-like scheme: comparison of the cumulus field with the different resolutions 256 × 257 (a, b) and 128 × 129 (c, d) at t = 44.8 days (a, c) and t = 46.7 days (b, d), starting from a same condition at t = 37.4 days. The format of the figure is same as in Fig. 5a. The size of the supercluster remains steady with the resolution 128 × 129 but decreases with 256 × 257.

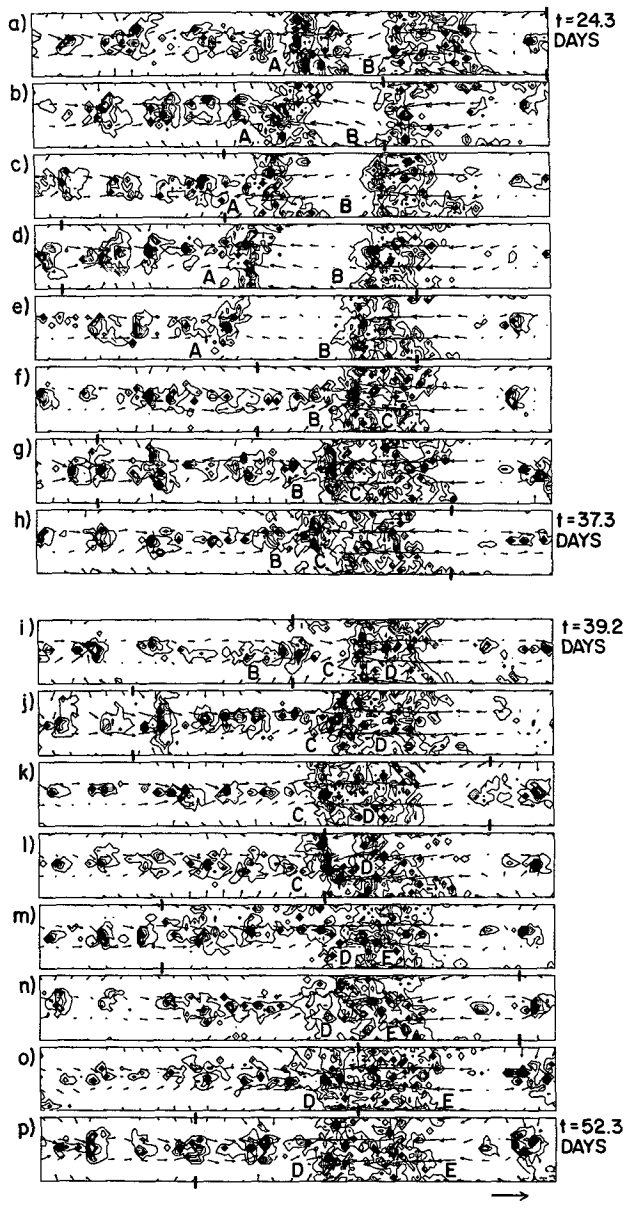

FIG. 19. A sequence of the generation and the decay of the superclusters within the Madden–Julian wave (with the grid-column scheme): from (a) t = 24.3 days after a restarting of the integration with 128 × 129 grids, to (p) t = 52.3 days with the interval of 1.87 days. The downdraft $\sigma_d w_d$ is shown with contour interval of 1.5 × 10^{-2} m s^{-1}. The minimum contour is 3 × 10^{-3} m s^{-1}. The wind vectors are shown with a unit scale 5 m s^{-1}. The area from 7.23°S to 7.23°N is shown with the frame moving with phase velocity 40 m s^{-1}, so that the center of the Madden–Julian wave remains at almost the same place in the frame. The origin in longitude (x = 0) is indicated by a pair of vertical bars along the latitudinal boundaries at each frame. The integration is initialized with an equilibrated state. The two superclusters A, B are seen at t = 24.3 days (a). The supercluster A gradually decays (a–d) and modulates into a cloud cluster (e), while a new supercluster C is generated east to the supercluster B at t = 33.6 days (f). Subsequently, the supercluster B decays and the supercluster C grows (g–h). By t = 39.2 days (i), the structure B is as weak as a cloud cluster, while the generation of a new supercluster D is noted. The pair of superclusters C, D survives until day 44.8 (l). Supercluster C is replaced by E by t = 46.7 days (m), which subsequently forms a pair with D (n–p).

field (Fig. 20a), while an increase of σ_c tends to generate gridpoint structures. With an extreme value σ_c = 0.1 (Fig. 20b), the result is virtually identical to that of the grid-column scheme, presumably because the convective ensembles then have a very short memory. A similar result is obtained when the convective downdrafts are completely turned off, *or* when 100% precipitation efficiency ϵ_p = 1.0 is assumed (Fig. 20c). On the other hand, if we decrease the precipitation efficiency ϵ_p, the cloud field becomes smoother and cloud clusters turn into a continuous tail of the supercluster (Fig. 20d).

6. Summary

A shallow-water analog of the tropical atmosphere on a constant SST ocean is proposed as a prototype to interpret the complex hierarchical structure of tropical disturbances. While the vertical resolution of the present model is crude, the very high horizontal resolution represents a substantial difference from earlier work (e.g., Lau and Peng 1987; Hendon 1988), and we have attempted to incorporate more realistic and physically plausible representations of convection and compare these with standard

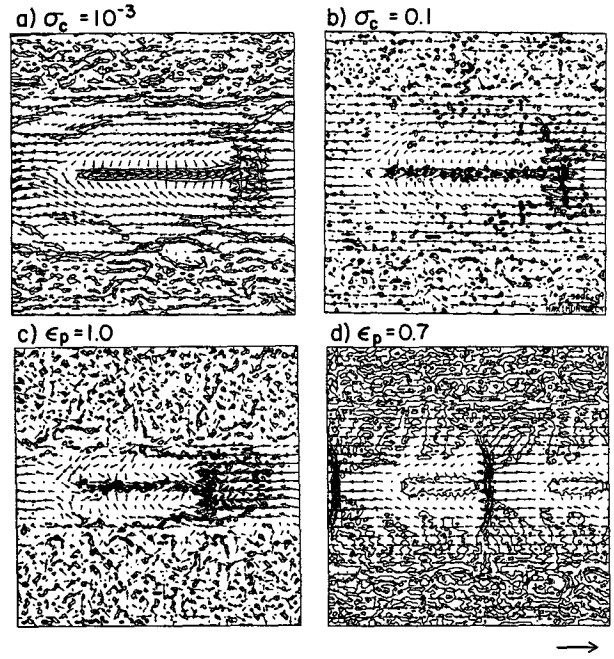

FIG. 20. The sensitivity of the dynamic-adjustment scheme to the downdraft effects: (a) with a small fractional cumulus area σ_c = 10^{-3} (t = 33.7 days); (b) with a large fractional cumulus area σ_c = 0.1 (t = 37.4 days); (c) without convective downdraft ϵ_p = 1.0 (t = 33.7 days); (d) with a strong convective downdraft ϵ_p = 0.7 (t = 33.7 days). The convective downdraft $\sigma_d w_d$ is plotted with the interval 6 × 10^{-4} m s^{-1} in (a) and (b), the cumulus updraft $\sigma_c w_c$ with the interval 6 × 10^{-3} m s^{-1} in (c), and convective downdraft is plotted with the interval 3 × 10^{-3} m s^{-1} in (d) with the minimum contour 6 × 10^{-4} m s^{-1}. A unit wind vector is 5 m s^{-1}. Compare with Figs. 2 and 5.

schemes. The model domain covers 180° in longitude on an equatorial β plane.

Model simulations using two different prognostic convective schemes and a Kuo-like scheme spontaneously generate a hierarchical convective structure, with eastward-propagating superclusters and westward-propagating cloud clusters when the imposed mean wind is not westerly;[3] simulations using a strict statistical equilibrium convection scheme fail to produce coherent, eastward-moving structures. The WISHE mechanism is identified as the source of the disturbances in all cases, although some structure does emerge with the Kuo scheme in the absence of WISHE.

Experiments with the four convective schemes show that the finite, albeit small, timescale of convection is crucial for good simulations of disturbances in the Tropics, and that downdrafts are important elements of convection that cannot be ignored. The lack of physical plausibility in Kuo-type schemes shows up as an aliasing of conditional instability onto the resolved scales and results in large sensitivity to grid size. It is also emphasized that the coincidence of the low-level convergence with the core of the superclusters as observed (e.g., Murakami and Nakazawa 1985) is obtained without assuming their direct coupling in the parameterization.

The qualitative behavior of disturbances in the equilibrated states conforms in most aspects to expectations based on linear theory. The dominant modes in the simulations using prognostic convective schemes consist of eastward-propagating planetary-scale structures of a Kelvin mode–like nature, and westward-moving synoptic-scale disturbances that more nearly resemble mixed Rossby–gravity waves in a westerly wind regime. This is also true, though to a lesser degree, with the Kuo scheme, but the imposition of strict statistical equilibrium eliminates any planetary wave structure, again in conformance with linear theory (Emanuel 1987). Also, the spatial structures of the superclusters resemble the linear response to a specified heat source (cf. Matsuno–Gill pattern).

Spatial inhomogeneity, in particular the longitudinal dependence of the sea surface temperature, is not required to generate a hierarchy of superclusters and cloud clusters, contrary to the suggestion of Lau et al. (1989). [Chao and Lin (1994) virtually share this conclusion, even though they did include a longitudinal dependence to the sea surface temperature.] The hierarchy is generated spontaneously through a series of coalescences of smaller cloud structures. The equilibrated kinetic energy is maximum at low wavenumbers. A somewhat surprising result is that nonlinear advection plays a secondary role in determining the nature of the equilibrated state. The most important nonlinearity in the model appears to be the switch that prevents convection in stable conditions. The power spectrum of convection and zonal wind in the fully nonlinear model is moderately well simulated by a reduced model in which the on/off switch in the convection scheme is the only remaining nonlinearity.

Two future directions of study with this type of the model are indicated. A gradual increase of the complexity of the model, with selective addition of features, such as a horizontal gradient of the sea surface temperature, land–sea contrast, and extratropical forcing, will help us understand the behavior of both more realistic models and the real atmosphere. It is also apparent that yet more work needs to be done to understand and mimic formation of convective ensemble and their interaction with the large-scale flow.

Acknowledgments. JIY appreciates conversations with A. Kasahara, J. Tribbia, and R. Milliff. Dick Valent and Paul Swarztrauber provided us a new two-dimensional FFT code for the present computations. JIY was supported by the NOAA Climate and Global Change Program.

APPENDIX

Summary of Symbols

a. Dry entropy

S_d ($\equiv \ln\theta$): dry entropy of the lower troposphere

Note that the factor C_p is omitted in the definition of entropies in this paper.

b. Equivalent entropy

S_{eb} ($\equiv \ln\theta_{eb}$): equivalent entropy of the subcloud layer

S_{em} ($\equiv \ln\theta_{em}$): equivalent entropy at the middle troposphere

S^*_{eb} ($\equiv \ln\theta^*_{eb}$): equivalent saturated entropy of the subcloud layer

S^*_{em} ($\equiv \ln\theta^*_{em} = \gamma S_d$): equivalent saturated entropy at the middle troposphere [cf. appendix of Emanuel (1987)]

c. Velocities

$\mathbf{v}_H$: horizontal wind velocity

w: vertical velocity at the middle troposphere

w_c: cumulus convective velocity (average over the grid scale)

w_d: downdraft velocity (average over the grid scale)

w_e: environmental subsidence (average over the grid scale)

d. Constants

1) THERMODYNAMICAL

$N = 10^{-2}\ \mathrm{s}^{-1}$: Brunt–Väisälä frequency

Γ_d: adiabatic lapse rate

[3] In contrast, the recent longitudinally one-dimensional experiment by Chao and Lin (1994) represents a strong cumulus parameterization dependence. The reason for such a strong dependence warrants further analysis, though this may well indicate the limitation of our approach with a vertically limited resolution.

$\Gamma_m = 6 \times 10^{-3}$ K/m: moist lapse rate
$\gamma = \Gamma_d/\Gamma_m = 1.7$
$T_b = 300$ K: temperature at the top of subcloud layer
$\bar{T}$: mean temperature over the troposphere
$\epsilon = (T_b - \bar{T})/T_b = 0.1$
$C_p = 10^3$ J/K·Kg: specific heat with constant pressure

2) RADIATIVE

$\tau_R = 50$ day: longwave radiative relaxation time (constant for Newtonian cooling term)
$\dot{Q}_{R0} = 4 \times 10^{-8}$ 1/s: constant cooling rate of the atmosphere by longwave radiation [corresponding to 1 K/day: Dopplick (1972, 1974)]

3) CLOUD PHYSICS

$\tau_d = 1.8$ hours: decaying timescale of downdrafts
σ_c: fractional area occupied by cumulus clouds in a single grid box ($\sigma_c = 0.01$ for the dynamic-adjustment scheme, $\sigma_c = 1.26 \times 10^{-3}$ for the grid-column scheme)
σ_d: fractional area covered by the downdrafts in a single grid box
ϵ_p: precipitation efficiency coefficient ($\epsilon_p = 1.0$ for the grid-column scheme, $\epsilon_p = 0.9$ for the statistical equilibrium and the dynamic-adjustment schemes)
B_c: critical buoyancy $B \equiv C_p\Gamma_m(S_{eb} - \gamma S_d)$ necessary to initiate cumulus convection in grid-column representation (assumed proportional to σ_c with $B_c = 1.5 \times 10^{-4}$ for the standard resolution $\Delta x = 161$ km)

4) DYNAMICAL

$\delta\phi$: perturbation geopotential
$\beta = 2.3 \times 10^{-8}$ s^{-1} K m^{-1}: equatorial beta parameter
$C_\theta = 1.2 \times 10^{-3}$: evaporation rate by wind
$C_D = 1 \times 10^{-3}$: surface drag coefficient
$\tau_D = 75$ days: Rayleigh forcing timescale
$u_0 = -10$ m s^{-1}: Rayleigh forcing wind

5) VERTICAL SCALES

$h = 500$ m: depth of subcloud layer
$H = 8$ km: depth of troposphere (density-weighted scale in log$p$ coordinate)
$H_m = 5$ km: height of middle-level troposphere (a level of minimum equivalent entropy, which is given by S_{em})

REFERENCES

Arakawa, A., and W. H. Schubert, 1974: Interaction of a cumulus cloud ensemble with the large-scale environment, Part I. *J. Atmos. Sci.*, **31,** 674–701.

——, and J.-M. Chen, 1986: Closure assumptions in the cumulus parameterization problem. *Proc. Symp. on Short- and Medium-Range Numerical Weather Prediction,* Tokyo, Japan, WMO/IUGG, 107–131.

Brown, R. G., and C. S. Bretherton, 1995: Tropical wave instabilities: Convective interaction with dynamics using the Emanuel convective parameterization. *J. Atmos. Sci.*, **52,** 67–82.

Chao, W. C., 1987: On the origin of the tropical intraseasonal oscillation. *J. Atmos. Sci.*, **44,** 1940–1949.

——, and S.-J. Lin, 1994: Tropical intraseasonal oscillation, super cloud clusters and cumulus convection schemes. *J. Atmos. Sci.*, **51,** 1282–1297.

Dopplick, T. G., 1972: Radiative heating of the global atmosphere. *J. Atmos. Sci.*, **29,** 1278–1294.

——, 1974: Global radiative heating in the atmosphere. *The General Circulation of the Tropical Atmosphere,* vol. 1, R. E. Newell, J. W. Kidson, B. G. Vincent, and G. J. Boer, Eds., MIT Press, 258 pp.

Durran, D. R., and J. B. Klemp, 1982: On the effects of moisture on the Brunt–Väisälä frequency. *J. Atmos. Sci.*, **39,** 2152–2158.

Emanuel, K. A., 1983: The Lagrangian parcel dynamics of moist symmetric instability. *J. Atmos. Sci.*, **40,** 2368–2376.

——, 1987: An air–sea interaction model of intraseasonal oscillations in the tropics. *J. Atmos. Sci.*, **44,** 2324–2340.

——, 1988: Reply. *J. Atmos. Sci.*, **45,** 3528–3530.

——, 1993: The effect of convective response time on WISHE modes. *J. Atmos. Sci.*, **50,** 1763–1775.

Gill, A. E., 1980: Some simple solutions for heat-induced tropical circulation. *Quart. J. Roy. Meteor. Soc.*, **106,** 447–462.

Hayashi, Y. Y., and A. Sumi, 1986: The 30–40 day oscillations simulated in an "aqua planet" model. *J. Meteor. Soc. Japan,* **64,** 451–467.

——, and T. Nakazawa, 1989: Evidence of the existence and eastward motion of super clusters. *Mon. Wea. Rev.*, **117,** 236–243.

Hendon, H. H., 1988: A simple model of the 40–50 day oscillation. *J. Atmos. Sci.*, **45,** 569–584.

Houze, R. A., Jr., 1989: Observed structure of mesoscale convective systems and implications for large-scale heating. *Quart. J. Roy. Meteor. Soc.*, **115,** 425–461.

Itoh, H., 1989: The mechanism for the scale-selection of tropical intraseasonal oscillations. Part I: Selection of wavenumber 1 and the three-scale structure. *J. Atmos. Sci.*, **46,** 1779–1798.

Krishnamurti, T. N., M. Kanamitsu, R. Godbole, C.-B. Chang, F. Carr, and J. H. Chow, 1976: Study of a monsoon depression. II: Dynamical structure. *J. Meteor. Soc. Japan,* **54,** 208–225.

——, Y. Ramanathan, H.-L. Pan, R. J. Pasch, and J. Molinari, 1980: Cumulus parameterization and rainfall rates, I. *Mon. Wea. Rev.*, **108,** 465–472.

Kuo, H. L., 1974: Further studies of the parameterization of the influence of cumulus convection on large-scale flow. *J. Atmos. Sci.*, **31,** 1232–1240.

Lau, K.-M., and L. Peng, 1987: Origin of low-frequency (intraseasonal) oscillation in the tropical atmosphere. *J. Atmos. Sci.*, **44,** 950–972.

——, ——, C. H. Sui, and T. Nakazawa, 1989: Dynamics of super clusters, westerly wind bursts, 30–60 day oscillations and ENSO: A unified view. *J. Meteor. Soc. Japan,* **67,** 205–219.

Leary, C. A., and R. A. Houze Jr., 1979: The structure and evolution of convection in a tropical cloud cluster. *J. Atmos. Sci.*, **36,** 437–457.

Lindzen, R., 1974: Wave–CISK in the tropics. *J. Atmos. Sci.*, **31,** 156–179.

Lovejoy, S., 1982: Area–perimeter relation for rain and cloud areas. *Science,* **216,** 185–187.

Madden, R. A., and P. R. Julian, 1971: Detection of a 40–50 day oscillation in the zonal wind in the tropical Pacific. *J. Atmos. Sci.*, **28,** 702–708.

——, and ——, 1972: Description of global-scale circulation cells in the tropics with a 40–50 day period. *J. Atmos. Sci.*, **29,** 1464–1469.

Matsuno, T., 1966a: Quasi-geostrophic motions in the equatorial area. *J. Meteor. Soc. Japan,* **44,** 25–43.

——, 1966b: Numerical integrations of the primitive equations by a simulated backward difference method. *J. Meteor. Soc. Japan,* **44,** 76–84.

Murakami, T., and T. Nakazawa, 1985: Tropical 45-day oscillation during the 1979 Northern Hemisphere summer. *J. Atmos. Sci.*, **42,** 1107–1122.

Nakazawa, T., 1988: Tropical super clusters within intraseasonal variations over the western Pacific. *J. Meteor. Soc. Japan,* **66,** 823–839.

Neelin, J. D., and J. Yu, 1994: Modes of tropical variability under convective adjustment and the Madden–Julian oscillation. Part I: Analytical theory. *J. Atmos. Sci.,* **51,** 1876–1894.

Numaguti, A., and Y.-Y. Hayashi, 1991: Behavior of cumulus activity and the structure of circulations in an "aqua planet" model. Part I: The structure of the super clusters. *J. Meteor. Soc. Japan,* **69,** 541–561.

Orszag, 1971: Numerical simulation of incompressible flows within simple boundaries: Galerkin, spectral representation. *Stud. Appl. Math.,* **50,** 293–327.

Wang, B., 1988: Dynamics of tropical low-frequency waves: An analysis of the moist Kelvin wave. *J. Atmos. Sci.,* **45,** 883–901.

Xie, S.-P., A. Kubokawa, and K. Hanawa, 1993a: Evaporation–wind feedback and the organizing of tropical convection on the planetary scale. Part I: Quasi-linear instability. *J. Atmos. Sci.,* **50,** 3873–3883.

——, ——, and ——, 1993b: Evaporation–wind feedback and the organizing of tropical convection on the planetary scale. Part II: Nonlinear evolution. *J. Atmos. Sci.,* **50,** 3884–3893.

Yano, J. I., and Y. Takeuchi, 1987: The self-similarity of horizontal cloud pattern in the intertropical convergence zone. *J. Meteor. Soc. Japan,* **65,** 661–667.

——, and N. Nishi, 1989: The hierarchy and self-affinity of the time variability within the tropical atmosphere inferred from the NOAA OLR data. *J. Meteor. Soc. Japan,* **67,** 771–789.

——, and K. A. Emanuel, 1991: An improved model of the equatorial troposphere and its coupling with the stratosphere. *J. Atmos. Sci.,* **48,** 377–389.

Zipser, E. J., 1969: The role of unsaturated convective downdrafts in the structure and rapid decay of an equatorial disturbance. *J. Appl. Meteor.,* **8,** 799–814.